Post-buckling of functionally graded microplates under mechanical and thermal loads using isogeomertic analysis

Son Thai[a], Huu-Tai Thai[a,*], Thuc P. Vo[b,c,*], J. N. Reddy[d]

[a]*School of Engineering and Mathematical Sciences, La Trobe University, Bundoora, VIC 3086, Australia*
[b]*Department of Mechanical and Construction Engineering, Northumbria University, Ellison Place, Newcastle upon Tyne NE1 8ST, UK*
[c]*Institute of Research and Development, Duy Tan University, 03 Quang Trung, Da Nang, Vietnam*
[d]*Advanced Computational Mechanics Laboratory, Department of Mechanical Engineering, Texas A & M University, College Station, TX 77843-3123, USA*

Abstract

The present study uses the isogeometric analysis (IGA) to investigate the post-buckling behavior of functionally graded (FG) microplates subjected to mechanical and thermal loads. The modified a strain gradient theory with three length scale parameters is used to capture the size effect. The Reddy third-order shear deformation plate theory with the von Kámán nonlinearity (i.e., small strains and moderate rotations) is employed to describe the kinematics of the microplates. Material variations in the thickness direction of the plate are described using a rule of mixtures. In addition, material properties are assumed to be either temperature-dependent or temperature-independent. The governing equations are derived using the principle of virtual work, which are then discretized using the IGA approach, whereby a C^2-continuity requirement is fulfilled naturally and efficiently. To trace the post-buckling paths, Newton's iterative technique is utilized. Various parametric studies are conducted to examine the influences of material variations, size effects, thickness ratios, and boundary conditions on the post-buckling behavior of microplates.

Keywords: Isogeometric analysis; Post-buckling; Thermal effect; Modified strain gradient theory; Microplate; Functionally graded plate

1. Introduction

Functionally graded materials (FGMs) [1] are a new class of composite materials that have been employed in various engineering applications. The adoption of FGMs can eliminate interface problems and alleviate thermal stress concentrations in structural components, which are the major con-

*Corresponding authors at: School of Engineering and Mathematical Sciences, La Trobe University, Bundoora, VIC 3086, Australia (H.T. Thai); Department of Mechanical and Construction Engineering, Northumbria University, Ellison Place, Newcastle upon Tyne NE1 8ST, UK (T.P. Vo)

Email addresses: thaibaoson@gmail.com (Son Thai), tai.thai@latrobe.edu.au (Huu-Tai Thai), thuc.vo@northumbria.ac.uk (Thuc P. Vo), jnreddy@tamu.edu (J. N. Reddy)

cerns with conventional laminated composites. These desirable features of FGMs are naturally obtained since their materials vary smoothly and continuously as functions of position along certain spatial direction. In general, a FGM is made from two different material constituents, for example, ceramic and metal phases. The ceramic constituent is considered as a high temperature barrier, thanks to its low thermal conductivity, whereas the metal counterpart is more ductile to prevent fracture due to thermal stresses. In addition to the linear analysis of FG plates [2], a large number of studies have been devoted to investigate their post-buckling responses [3–18]. A comprehensive review of plate theories and techniques used to analyse FG plates subjected to mechanical and thermal loads can be found in [2, 19, 20].

In recent years, beams and plates whose dimensions are in microns and nanometers have been widely employed in advanced devices, such as microelectromechanical systems (MEMS) and nano electromechanical systems (NEMS). With the distinguishing features, the FGMs were also employed in such applications [21, 22]. In fact, the behaviour of small scale structures is considerably influenced by material size effects, which can only be captured using non-classical elasticity theories with length scale parameters. In the literature, nonlocal elasticity proposed by Eringen [23], Modified Couple stress Theory (MCT) of Yang et al. [24] and Modified Strain gradient Theory (MST) of Lam et al. [25] are widely used to investigate the behaviour of micro/nano structures. Recent studies on the developments and applications of nonlocal theory to nanobeams and nanopaltes could be found in the works of Li et al. [26–29], Nguyen et al. [30], and Phung-Van et al. [31]. Based on the MCT, numerous studies have been also carried out to investigate the behaviour of micro beams and plates [32–35, 35–45]. For nonlinear analysis in accordance with the MCT, Reddy and Kim [41] developed a model based on a general third-order shear deformation plate theory, which can be specialized to classical, first-order shear deformation, the Reddy third-order plate theories and accounts for both von Kármán nonlinearity and FGMs. Ke et al. [46, 47] also investigated the nonlinear free vibration of FG annular microplates and microbeams by adopting MCT. Based on the classical and first-order theory, Reddy et al. [48] presented finite element models of microstructure-dependent nonlinear theories for axisymmetric bending of FG circular plates, which account for the through-thickness power-law variation of a two-constituent materia, the von Kármán nonlinearity, and the couple stress effects. Compared to the MCT, the MST is more extensive and general in dealing with micro structures. In addition, the MST is less complicated in terms of mathematical formulations than the classical strain gradient theory [49], which can have more length scales. Therefore, various studies has been published in the literature to discuss the size effect in micro structures based on the MST. Wang et al. [50] and Ashoori Movassagh and Mahmoodi [51] developed the Navier solutions for bending, vibra-

tion, and buckling responses of isotropic microplates. Sahmani and Ansari [52] also employed the analytical approach to examine the free vibration behavior of FG microplates using higher-order plate theories. Kirchhoff's plate theory was adopted by Li et al. [53] to predict the bending response of bi-layer microplates. Ansari et al. [54] and Zhang et al. [55] derived the displacements, frequencies and buckling loads of annular/circular FG microplates. Zhang et al. [56] also developed an analytical model using the refined plate theory to investigate the response of FG microplates resting on an elastic foundation. The buckling and free vibration responses of FG microplates were also addressed in the the study of Mirsalehi et al. [57] by using the finite strip method. Hosseini et al. [58] employed an analytical approach to study the buckling responses of an orthotropic multi-microplate system embedded in an elastic medium. Thai et al. [59] also carried out a comprehensive investigation on linear bending, free vibration and buckling responses of FG microplates by using IGA approach. In addition, the behaviour of microplates under thermal loads was also examined based on the MST in some studies recently. For example, Ansari et al. [60] presented an investigation on the linear thermal buckling of FG microplates based on the first-order plate theory. Shenas and Malekzadeh [61] discussed the influence of thermal environment on the free vibration behavior of quadrilateral FG microplates by using the Chebyshev-Ritz method. Emami and Alibeigloo [62] also adopted the first-order plate theory and analytical approach to study the thermoelastic damping behavior of FG microplates, in which the coupled thermoelasticity was investigated together with the size effect.

A review of the literature [22] shows that there are very few studies on the post-buckling behavior of microplates based on the MST so far. From an analytical point of view, the post-buckling behavior of plate structures could be investigated using different approaches, such as analytical, semi-analytical, and numerical methods. The analytical approach is only suitable for the problems with simple geometries and boundary conditions, whereas other numerical methods encounter the difficulty in fulfilling the high-order continuity requirement of the interpolation functions, for example, when the first- or high-order shear deformation theory is considered. The IGA approach [63] which is known as advanced computational techniques have been extensively employed to deal with various problems in many fields of computational mechanics. The core idea of IGA is to employ the predominant technology used in Computer-Aided Design (CAD) as geometry discretization technique and discretization tool for analysis. Non-uniform rational B-splines functions inheriting the advanced features in geometrical modelling allow the IGA approach not only to be able to generate highly continuous interpolations but also present exactly the geometries of arbitrary conical shapes, hence the error in geometrical modelling could be alleviated. For shell and plate problems in particular, the smoothness of basis functions obtained from IGA approach allows the construction of plate/shell el-

ement less complicated compared to other techniques [64]. In addition, k-refinement which is unique to IGA presents a robust and systematic technique to elevate the continuity of interpolation functions efficiently and naturally.

In this study, the post-buckling behavior of FG microplates under mechanical or thermal loads is investigated using IGA-based numerical model and the MST. The shear deformation effect is also investigated using the Reddy third-order shear deformation theory [65]. The von Kámán nonlinear strains and temperature dependent properties are accounted for. The principle of virtual work is utilized to derive the weak form equation of the problem. Based on the IGA technique, the C^2-continuity of the interpolation functions is met naturally and efficiently. The post-buckling paths are traced using Newton's iterative procedure with small initial imperfection. Verification exercises are performed to present the accuracy of the present approach. In addition, various parametric studies are carried out to determine the influences of the power-law indices, size effects, thickness ratios, and boundary conditions on the post-buckling response of FG microplates.

2. Material properties of FGMs

For a FG rectangular plate whose geometry and coordinates are depicted in Fig. 1, the material properties such as Young's modulus $E(z)$, thermal conductivity $\kappa(z)$, and thermal expansion $\alpha(z)$ vary throughout the thickness h according to the rule of mixture as [3]

$$P\left(z\right) = \left(P_c - P_m\right)\left(\frac{z}{h} + \frac{1}{2}\right)^n + P_m \tag{1}$$

where c and m indicate ceramic and metal and n is the material gradient index. A purely ceramic or metal plate is obtained by setting n = 0 or $n = \infty$, respectively.

For the temperature-dependent materials, their properties are calculated by [66]

$$P = P_0\left(P_{-1}T^{-1} + 1 + P_1T^1 + P_2T^2 + P_3T^3\right) \tag{2}$$

where P_0, P_{-1}, P_1, P_2 and P_3 are the temperature coefficients. In this study, the temperature is assumed to vary only throughout the thickness. Uniform temperature rise and nonlinear temperature rise are taken into consideration. In addition, it is assumed that there is no internal heat generation within the plate's volume.

In the case of uniform temperature rise, the temperature of whole plate is assumed to be uniform and increase from the referenced temperature T_0 = 300^0K to prescribed values. In other words, the temperature at any point in the plate is $T\left(z\right) = T_0 + \Delta T$ with ΔT being the increment of temperature.

When the nonlinear temperature rise is considered, the temperature distribution along the thickness direction is based on the one-dimensional steady-state heat conduction equation, with related

boundary conditions, as follows:

$$\frac{d}{dz}\left[\kappa\left(z\right)\frac{dT}{dz}\right]=0;\ T|_{z=-h/2}=T_m=300^0K;\ T|_{z=h/2}=T_c=T_m+\Delta T \tag{3}$$

The solutions of the above equation are obtained using the polynomial series [67] as follows:

$$T\left(z\right)=T_m+\frac{T_c-T_m}{C}\left[V_f-\frac{\kappa_{cm}}{\left(n+1\right)\kappa_m}V_f^{n+1}+\frac{\kappa_{cm}^2}{\left(2n+1\right)\kappa_m^2}V_f^{2n+1}-\frac{\kappa_{cm}^3}{\left(3n+1\right)\kappa_m^3}V_f^{3n+1}\right.$$
$$\left.+\frac{\kappa_{cm}^4}{\left(4n+1\right)\kappa_m^4}V_f^{2n+1}-\frac{\kappa_{cm}^5}{\left(5n+1\right)\kappa_m^5}V_f^{5n+1}\right] \tag{4}$$

where $V_f=\frac{1}{2}+\frac{z}{h}$, $\kappa_{cm}=\kappa_c-\kappa_m$, and

$$C=1-\frac{\kappa_{cm}}{\left(n+1\right)\kappa_m}+\frac{\kappa_{cm}^2}{\left(2n+1\right)\kappa_m^2}-\frac{\kappa_{cm}^3}{\left(3n+1\right)\kappa_m^3}+\frac{\kappa_{cm}^4}{\left(4n+1\right)\kappa_m^4}-\frac{\kappa_{cm}^5}{\left(5n+1\right)\kappa_m^5} \tag{5}$$

3. Size-dependent plate formulation

3.1. Modified strain gradient theory (MST)

In the MST proposed by Lam et al. [25], the virtual strain energy stored in an elastic body depends not only on the conventional strain but also on the other high-order strain gradients:

$$\delta U=\int_V\left(\sigma_{ij}\delta\varepsilon_{ij}+p_i\delta\varsigma_i+\tau_{ijk}^{(1)}\delta\eta_{ijk}^{(1)}+m_{ij}^s\delta\chi_{ij}^s\right)dV \tag{6}$$

where ε_{ij} is the classical strain tensor, ζ_i is the dilatation gradient tensor, $\eta_{ijk}^{(1)}$ is the deviatoric stretch gradient tensor, and χ_{ij}^s is the symmetric part of rotation gradient tensor. Their definitions are given as follows:

$$\varepsilon_{ij}=\frac{1}{2}\left(u_{i,j}+u_{j,i}+u_{m,i}u_{m,j}\right) \tag{7a}$$

$$\varsigma_i=\varepsilon_{mm,i} \tag{7b}$$

$$\eta_{ijk}^{(1)}=\frac{1}{3}\left(\varepsilon_{jk,i}+\varepsilon_{ki,j}+\varepsilon_{ij,k}\right)-$$
$$\frac{1}{15}\delta_{ij}\left(\varepsilon_{mm,k}+2\varepsilon_{mk,m}\right)-\frac{1}{15}\delta_{jk}\left(\varepsilon_{mm,i}+2\varepsilon_{mi,m}\right)-\frac{1}{15}\delta_{ki}\left(\varepsilon_{mm,j}+2\varepsilon_{mj,m}\right) \tag{7c}$$

$$\chi_{ij}^s=\frac{1}{4}\left(e_{imn}u_{n,mj}+e_{jmn}u_{n,mi}\right) \tag{7d}$$

where u_i are the components of displacement vector; δ_{ij} and e_{ijk} are the Kronocker delta and permutation symbol, respectively. The constitutive relations for classical stresses (σ_{ij}) and high-order stresses $(p_i, \tau_{ijk}^{(1)}$, and $m_{ij}^s)$ are expressed as follows:

$$\sigma_{ij}=2\mu\varepsilon_{ij}+\lambda\varepsilon_{kk}\delta_{ij}-\alpha\left(3\lambda+2\mu\right)\Delta T\delta_{ij} \tag{8a}$$

$$p_i = 2\mu l_0^2 \varsigma_i \tag{8b}$$

$$\tau_{ijk}^{(1)} = 2\mu l_1^2 \eta_{ijk}^{(1)} \tag{8c}$$

$$m_{ij}^s = 2\mu l_2^2 \chi_{ij}^s \tag{8d}$$

where l_0, l_1, and l_2 are three material length scale parameters and λ and μ are the Lamé constants

$$\lambda = \frac{\nu(z)E(z)}{[1+\nu(z)]\,[1-2\nu(z)]};\;\; \mu = \frac{E(z)}{2\,[1+\nu(z)]} \tag{9}$$

It should be noted in Eq. (8) that the thermal effect is assumed to be only accounted for in the classical stress [60, 61]. When the coupled thermoelastic problems and thickness stretching effect are considered, the high-order stresses corresponding to the dilatation gradient tensor p_i should be modified. More information about this aspect can be found in [62, 68].

3.2. Kinematic formulation

Based on the the Reddy third-order shear deformation theory [65], the displacement field of plates is described by

$$\left\{\begin{array}{c} u_1 \\ u_2 \\ u_3 \end{array}\right\} = \left\{\begin{array}{c} u \\ v \\ w \end{array}\right\} + f\,(z) \left\{\begin{array}{c} \theta_x \\ \theta_y \\ 0 \end{array}\right\} - g\,(z) \left\{\begin{array}{c} w_{,x} \\ w_{,y} \\ 0 \end{array}\right\} \tag{10}$$

in which (u, v, w) and (θ_x, θ_y) denote the displacements and rotations of transverse normals at an arbitrary point in the middle surface Ω; $f\,(z) = z - 4z^3/3h^2$ and $g\,(z) = 4z^3/3h^2$

By substituting Eq. (10) into Eq. (7), the strain-displacement relationships based on the von Kármán nonlinearity are obtained as follows:

$$\boldsymbol{\varepsilon} = \boldsymbol{\varepsilon}_0 + \frac{1}{2}\boldsymbol{\varepsilon}_{nl} + f\,(z)\,\boldsymbol{\varepsilon}_1 + g\,(z)\,\boldsymbol{\varepsilon}_2;\;\; \boldsymbol{\gamma} = f'\,(z)\,\boldsymbol{\gamma}_1 + (1 - g'\,(z))\,\boldsymbol{\gamma}_2 \tag{11a}$$

$$\boldsymbol{\varsigma} = \boldsymbol{\varsigma}_0 + \boldsymbol{\varsigma}_{nl} + f\,(z)\,\boldsymbol{\varsigma}_1 + g\,(z)\,\boldsymbol{\varsigma}_2;\; \varsigma_z = f'\,(z)\,\varsigma_3 + g'\,(z)\,\varsigma_4 \tag{11b}$$

$$\boldsymbol{\eta} = \boldsymbol{\eta}_0 + \boldsymbol{\eta}_{nl} + f''\,(z)\,\boldsymbol{\eta}_1 + f'\,(z)\,\boldsymbol{\eta}_2 + f\,(z)\,\boldsymbol{\eta}_3 + g''\,(z)\,\boldsymbol{\eta}_4 + g'\,(z)\,\boldsymbol{\eta}_5 + g\,(z)\,\boldsymbol{\eta}_6 \tag{11c}$$

$$\boldsymbol{\chi} = \boldsymbol{\chi}_0 + f''\,(z)\,\boldsymbol{\chi}_1 + f'\,(z)\,\boldsymbol{\chi}_2 + f\,(z)\,\boldsymbol{\chi}_3 + g''\,(z)\,\boldsymbol{\chi}_4 + g'\,(z)\,\boldsymbol{\chi}_5 \tag{11d}$$

Here, the primes represent derivatives with respect to z. In addition, it is observed that the nonlinearity is contributed from the classical strain tensor, dilatation gradient tensor, and deviatoric stretch gradient tensor, whereas the symmetric part of rotation gradient tensor has no nonlinear component. The details of those quantities are given in Appendix A.

The constitutive equations of size-dependent third-order shear deformation plates can be expressed in terms of stress resultants by substituting Eq. (11) into Eq. (8) as follows:

$$\hat{\boldsymbol{\sigma}} = \hat{\mathbf{D}}_\varepsilon \left(\hat{\boldsymbol{\varepsilon}} + \frac{1}{2}\boldsymbol{\varepsilon}_{nl}\right) - \hat{\boldsymbol{\sigma}}_T \tag{12a}$$

$$\hat{\mathbf{p}} = \hat{\mathbf{D}}_{\varsigma}\left(\hat{\boldsymbol{\varsigma}} + \boldsymbol{\varsigma}_{nl}\right) \tag{12b}$$

$$\hat{\boldsymbol{\tau}} = \hat{\mathbf{D}}_{\eta}\left(\hat{\boldsymbol{\eta}} + \boldsymbol{\eta}_{nl}\right) \tag{12c}$$

$$\hat{\mathbf{m}} = \hat{\mathbf{D}}_{\chi}\hat{\boldsymbol{\chi}} \tag{12d}$$

where $\hat{\mathbf{D}}_{\varepsilon}, \hat{\mathbf{D}}_{\varsigma}, \hat{\mathbf{D}}_{\eta}$ and $\hat{\mathbf{D}}_{\chi}$ are the constituent matrices whose definitions are presented in Appendix B,

$$\hat{\boldsymbol{\varepsilon}} = \begin{Bmatrix} \boldsymbol{\varepsilon}_0 \\ \boldsymbol{\varepsilon}_1 \\ \boldsymbol{\varepsilon}_2 \\ \boldsymbol{\gamma}_1 \\ \boldsymbol{\gamma}_2 \end{Bmatrix};\ \boldsymbol{\varepsilon}_{nl} = \begin{Bmatrix} \boldsymbol{\varepsilon}_{nl} \\ \mathbf{0} \\ \mathbf{0} \\ \mathbf{0} \\ \mathbf{0} \end{Bmatrix};\ \hat{\boldsymbol{\varsigma}} = \begin{Bmatrix} \boldsymbol{\varsigma}_0 \\ \boldsymbol{\varsigma}_1 \\ \boldsymbol{\varsigma}_2 \\ \boldsymbol{\varsigma}_3 \\ \boldsymbol{\varsigma}_4 \end{Bmatrix};\ \boldsymbol{\varsigma}_{nl} = \begin{Bmatrix} \boldsymbol{\varsigma}_{nl} \\ \mathbf{0} \\ \mathbf{0} \\ \mathbf{0} \\ \mathbf{0} \end{Bmatrix} \tag{13a}$$

$$\hat{\boldsymbol{\eta}} = \begin{Bmatrix} \boldsymbol{\eta}_0 \\ \boldsymbol{\eta}_1 \\ \boldsymbol{\eta}_2 \\ \boldsymbol{\eta}_3 \\ \boldsymbol{\eta}_4 \\ \boldsymbol{\eta}_5 \\ \boldsymbol{\eta}_6 \end{Bmatrix};\ \boldsymbol{\eta}_{nl} = \begin{Bmatrix} \boldsymbol{\eta}_{nl} \\ \mathbf{0} \\ \mathbf{0} \\ \mathbf{0} \\ \mathbf{0} \\ \mathbf{0} \\ \mathbf{0} \end{Bmatrix};\ \hat{\boldsymbol{\chi}} = \begin{Bmatrix} \boldsymbol{\chi}_0 \\ \boldsymbol{\chi}_1 \\ \boldsymbol{\chi}_2 \\ \boldsymbol{\chi}_3 \\ \boldsymbol{\chi}_4 \\ \boldsymbol{\chi}_5 \end{Bmatrix} \tag{13b}$$

and $\hat{\boldsymbol{\sigma}}_T$ is the thermal stress resultant, which is given by

$$\hat{\boldsymbol{\sigma}}_T = \int_{-h/2}^{h/2} \Delta T\left(z\right) \begin{Bmatrix} \tilde{\mathbf{Q}}_b \\ f\left(z\right)\tilde{\mathbf{Q}}_b \\ g\left(z\right)\tilde{\mathbf{Q}}_b \\ \mathbf{0} \\ \mathbf{0} \end{Bmatrix} dz;\ \tilde{\mathbf{Q}}_b = \mathbf{Q}_b \begin{Bmatrix} \alpha\left(z\right) \\ \alpha\left(z\right) \\ 0 \end{Bmatrix} \tag{14}$$

By adopting the small strain assumption, the governing equation of the postbucking problem obtained from the principle of virtual work can be expressed with respect to the initial configuration as

$$\begin{aligned} \int_{\Omega} \delta\left(\hat{\boldsymbol{\varepsilon}} + \frac{1}{2}\boldsymbol{\varepsilon}_{nl}\right)^T \left[\hat{\mathbf{D}}_{\varepsilon}\left(\hat{\boldsymbol{\varepsilon}} + \frac{1}{2}\boldsymbol{\varepsilon}_{nl}\right) - \hat{\boldsymbol{\sigma}}_T\right] d\Omega + \int_{\Omega} \delta(\hat{\boldsymbol{\varsigma}} + \boldsymbol{\varsigma}_{nl})^T \hat{\mathbf{D}}_{\varsigma}\left(\hat{\boldsymbol{\varsigma}} + \boldsymbol{\varsigma}_{nl}\right) d\Omega \\ + \int_{\Omega} \delta(\hat{\boldsymbol{\eta}} + \boldsymbol{\eta}_{nl})^T \hat{\mathbf{D}}_{\eta}\boldsymbol{\Gamma}_{\eta}\left(\hat{\boldsymbol{\eta}} + \boldsymbol{\eta}_{nl}\right) d\Omega + \int_{\Omega} \delta\hat{\boldsymbol{\chi}}^T \hat{\mathbf{D}}_{\chi}\boldsymbol{\Gamma}_{\chi}\hat{\boldsymbol{\chi}} d\Omega = \int_{\Gamma} \delta\mathbf{u}^T \hat{\mathbf{t}} d\Gamma \end{aligned} \tag{15}$$

where $\hat{\mathbf{t}}$ is the traction force applied in the boundary Γ and $\mathbf{u} = \left\{ \begin{array}{ccccc} u & v & \theta_x & \theta_y & w \end{array} \right\}^T$ is the displacement vector. $\boldsymbol{\Gamma}_{\eta}$ and $\boldsymbol{\Gamma}_{\chi}$ are the diagonal matrices of coefficients

$$diag\left(\boldsymbol{\Gamma}_{\eta}\right) = \left\{ \begin{array}{ccccccccccc} 1 & 1 & 1 & 3 & 3 & 3 & 6 & 1 & 1 & 1 \end{array} \right\} \tag{16a}$$

$$diag\left(\mathbf{\Gamma}_{\chi}\right)=\left\{\begin{array}{cccccc}1 & 1 & 2 & 1 & 2 & 2\end{array}\right\} \tag{16b}$$

4. Isogeometric Analysis

By using the IGA approach [69, 70], the displacement variables are interpolated as follows

$$\mathbf{u}=\sum_{c}^{m\times n}R_{c}\left(\xi,\eta\right)\mathbf{d}_{c} \tag{17}$$

where vector $\mathbf{d}_{c}=\left\{\begin{array}{ccccc}u_{c} & v_{c} & \theta_{xc} & \theta_{yc} & w_{c}\end{array}\right\}^{T}$ consists the corresponding variables at control point c, $m\times n$ denotes the numbers of control points associated in an element, and R_{c} are the 2-dimensional B-splines basis functions. Substituting Eq. (17) into Eq. (12), the relationships between strains ans and displacements are given as follows

$$\hat{\boldsymbol{\varepsilon}}=\sum_{c}^{m\times n}\mathbf{B}_{\varepsilon c}\mathbf{d}_{c};\ \boldsymbol{\varepsilon}_{nl}=\sum_{c}^{m\times n}\mathbf{B}_{\varepsilon nl}\mathbf{d}_{c}=\sum_{c}^{m\times n}\mathbf{\Lambda}_{\varepsilon c}\mathbf{B}_{gc}\mathbf{d}_{c} \tag{18a}$$

$$\hat{\boldsymbol{\varsigma}}=\sum_{c}^{m\times n}\mathbf{B}_{\varsigma c}\mathbf{d}_{c};\ \boldsymbol{\varsigma}_{nl}=\sum_{c}^{m\times n}\mathbf{B}_{\varsigma nl}\mathbf{d}_{c}=\sum_{c}^{m\times n}\mathbf{\Lambda}_{\varsigma c}\mathbf{B}_{gc}\mathbf{d}_{c} \tag{18b}$$

$$\hat{\boldsymbol{\eta}}=\sum_{c}^{m\times n}\mathbf{B}_{\eta c}\mathbf{d}_{c};\ \boldsymbol{\eta}_{nl}=\sum_{c}^{m\times n}\mathbf{B}_{\eta nl}\mathbf{d}_{c}=\sum_{c}^{m\times n}\mathbf{\Lambda}_{\eta c}\mathbf{B}_{gc}\mathbf{d}_{c} \tag{18c}$$

$$\hat{\boldsymbol{\chi}}=\sum_{c}^{m\times n}\mathbf{B}_{\chi c}\mathbf{d}_{c} \tag{18d}$$

Details of the strain-displacement matrices are presented explicitly in Appendix C.

The equations for the post-buckling problems of FG microplates subjected to mechanical and thermal loadings are obtained by substituting Eqs. (18) into the weak form in Eq. (15) as follows

$$\left(\mathbf{K}_{\varepsilon m}+\mathbf{K}_{\varsigma}+\mathbf{K}_{\eta}+\mathbf{K}_{\chi}\right)\mathbf{d}=\mathbf{f}_{m} \tag{19a}$$

$$\left(\mathbf{K}_{\varepsilon t}+\mathbf{K}_{\varsigma}+\mathbf{K}_{\eta}+\mathbf{K}_{\chi}\right)\mathbf{d}=\mathbf{f}_{t} \tag{19b}$$

where $\mathbf{K}_{\varepsilon m}$ and $\mathbf{K}_{\varepsilon t}$ are stiffness matrices corresponding to the classical strain tensor ε_{ij} when the mechanical and thermal loadings are considered, respectively. $\mathbf{K}_{\varsigma}, \mathbf{K}_{\eta}$ and $\mathbf{K}_{\chi}$ are the stiffness matrices related to the dilatation gradient tensor ς_{i}, deviatoric stretch gradient tensor $\eta_{ijk}^{(1)}$ and symmetric part of rotation gradient tensor χ_{ij}^{s}, respectively.

$$\mathbf{K}_{\varepsilon m}=\int_{\Omega}\left(\mathbf{B}_{\varepsilon T}^{T}\hat{\mathbf{D}}_{\varepsilon}\mathbf{B}_{\varepsilon}+\frac{1}{2}\mathbf{B}_{\varepsilon T}^{T}\hat{\mathbf{D}}_{\varepsilon}\mathbf{B}_{\varepsilon nl}+\mathbf{B}_{\varepsilon nl}^{T}\hat{\mathbf{D}}_{\varepsilon}\mathbf{B}_{\varepsilon}+\frac{1}{2}\mathbf{B}_{\varepsilon nl}^{T}\hat{\mathbf{D}}_{\varepsilon}\mathbf{B}_{\varepsilon nl}\right)d\Omega \tag{20a}$$

$$\mathbf{K}_{\varepsilon t}=\int_{\Omega}\left(\mathbf{B}_{\varepsilon T}^{T}\hat{\mathbf{D}}_{\varepsilon}\mathbf{B}_{\varepsilon}+\frac{1}{2}\mathbf{B}_{\varepsilon T}^{T}\hat{\mathbf{D}}_{\varepsilon}\mathbf{B}_{\varepsilon nl}+\mathbf{B}_{\varepsilon nl}^{T}\hat{\mathbf{D}}_{\varepsilon}\mathbf{B}_{\varepsilon}+\frac{1}{2}\mathbf{B}_{\varepsilon nl}^{T}\hat{\mathbf{D}}_{\varepsilon}\mathbf{B}_{\varepsilon nl}-\mathbf{B}_{g}^{T}\hat{\mathbf{N}}_{th}\mathbf{B}_{g}\right)d\Omega \tag{20b}$$

$$\mathbf{K}_{\varsigma} = \int_{\Omega} \left(\mathbf{B}_{\varsigma T}^{T} \hat{\mathbf{D}}_{\varsigma} \mathbf{B}_{\varsigma} + \mathbf{B}_{\varsigma T}^{T} \hat{\mathbf{D}}_{\varsigma} \mathbf{B}_{\varsigma nl} + \mathbf{B}_{\varsigma nl}^{T} \hat{\mathbf{D}}_{\varsigma} \mathbf{B}_{\varsigma} + \mathbf{B}_{\varsigma nl}^{T} \hat{\mathbf{D}}_{\varsigma} \mathbf{B}_{\varsigma nl} + \mathbf{B}_{g}^{T} \hat{\mathbf{N}}_{\varsigma} \mathbf{B}_{g\varsigma} \right) d\Omega \tag{20c}$$

$$\mathbf{K}_{\eta} = \int_{\Omega} \left(\mathbf{B}_{\eta T}^{T} \mathbf{\Gamma}_{\eta} \hat{\mathbf{D}}_{\eta} \mathbf{B}_{\eta} + \mathbf{B}_{\eta T}^{T} \mathbf{\Gamma}_{\eta} \hat{\mathbf{D}}_{\eta} \mathbf{B}_{\eta nl} + \mathbf{B}_{\eta nl}^{T} \mathbf{\Gamma}_{\eta} \hat{\mathbf{D}}_{\eta} \mathbf{B}_{\eta} + \mathbf{B}_{\eta nl}^{T} \mathbf{\Gamma}_{\eta} \hat{\mathbf{D}}_{\eta} \mathbf{B}_{\eta nl} + \mathbf{B}_{g}^{T} \hat{\mathbf{N}}_{\eta} \mathbf{B}_{g\eta} \right) d\Omega \tag{20d}$$

$$\mathbf{K}_{\chi} = \int_{\Omega} \mathbf{B}_{\chi T}^{T} \hat{\mathbf{D}}_{\chi} \mathbf{\Gamma}_{\chi} \mathbf{B}_{\chi} \mathbf{d} d\Omega \tag{20e}$$

$\mathbf{f}_m$ and $\mathbf{f}_m$ are the force vectors due to mechanical and thermal loadings

$$\mathbf{f}_m = \int_{\Gamma} \mathbf{B}_{\Gamma}^{T} \hat{\mathbf{t}} d\Gamma; \mathbf{f}_t = \int_{\Omega} \mathbf{B}_{\varepsilon T}^{T} \hat{\boldsymbol{\sigma}}_T d\Omega \tag{21}$$

where $\mathbf{B}_{\Gamma} = \begin{Bmatrix} R_{\Gamma} & R_{\Gamma} & 0 & 0 & 0 \end{Bmatrix}$ with R_{Γ} being the 1D basis function defined along the boundary of the plate.

It can be seen from the IGA-based formulations (see Appendix C) that the third-order derivatives of basis functions are required for constructing stiffness matrices. Consequently, the basis functions with C^2-continuity over the parametric space are needed. In general, this requirement is not easy to handle when it is considered within the basis of traditional finite element approach. As mentioned earlier, the basis functions obtained from the IGA approach are able to provide highly continuous interpolations naturally and efficiently thanks to an advanced $k-$refinement technique [70]. For C^2-continuous interpolations, the basis functions with order of p = 3 are employed in this study.

5. Solution procedures

In general, the post-buckling problems considered within the framework of numerical methods could be classified into two types: nonlinear eigenvalue analysis and geometrically nonlinear analysis. The nonlinear eigenvalue analysis is applicable to solve the post-buckling problems when the bifurcation buckling does happen. In other words, the plate still remains its initial configuration under the effects of compressive or thermal loadings until the buckling phenomenon takes place with sudden deformations. In general, the bifurcation buckling occurs when the plate is perfectly flat and only membrane forces are generated under the effects of external loadings. In case the plate is subjected to mechanical loadings, the latter condition is obtained when the plates are made from homogeneous materials or symmetric angle-fly laminated composites. When the plates are imposed to thermal effects, the bifurcation buckling only takes place with uniform temperature rise and the aforementioned conditions of materials are satisfied. However, when those conditions are violated, the bifurcation buckling still occurs when the clamped boundary conditions are considered. This is

due to the fact that this type of boundary condition is capable of preventing the plates from deforming suddenly under the effects of coupling or thermal moments. The general procedure of nonlinear eigenvalue analysis was presented in the papers of Liew et al. [71] and Tran et al. [16]. When the conditions for bifurcation buckling to occur are not satisfied (e.g. the the plates is made from inhomogeneous plates such as FGMs, unsymmetrically laminated composites, the temperature dose not vary throughout the thickness uniformly, or when the clamped boundary condition is not considered), the plate would deform immediately as soon as the external loads are imposed due to extension-bending coupling effects. As a result, the nonlinear eigenvalue analysis cannot represent the stability status of the plates correctly in such cases and the geometrically nonlinear analysis is therefore needed to be conducted to obtained accurate results. In addition, it is possible to capture the bifurcation buckling with geometrically nonlinear analysis by imposing a relatively small imperfection on the initial geometry of the plates. Therefore, the latter approach is employed in this study to investigate the post-buckling behaviour of FG microplates. Herein, the post-buckling paths are traced using the Newton's iterative technique, in which the deformed geometry of the first mode in linear buckling analysis is imposed as a small initial imperfection [72]. The tangent stiffness matrix of the present model is given by

$$\mathbf{K}_T = \mathbf{K}_{T\varepsilon} + \mathbf{K}_{T\varsigma} + \mathbf{K}_{T\eta} + \mathbf{K}_{\chi} \tag{22}$$

where

$$\mathbf{K}_{T\varepsilon} = \int_{\Omega} \left(\mathbf{B}_{\varepsilon T}^T \hat{\mathbf{D}}_{\varepsilon} \mathbf{B}_{\varepsilon} + \mathbf{B}_{\varepsilon T}^T \hat{\mathbf{D}}_{\varepsilon} \mathbf{B}_{\varepsilon nl} + \mathbf{B}_{\varepsilon nl}^T \hat{\mathbf{D}}_{\varepsilon} \mathbf{B}_{\varepsilon} + \mathbf{B}_{\varepsilon nl}^T \hat{\mathbf{D}}_{\varepsilon} \mathbf{B}_{\varepsilon nl} + \mathbf{B}_g^T \hat{\mathbf{N}}_{\varepsilon} \mathbf{B}_g \right) d\Omega \tag{23a}$$

$$\mathbf{K}_{T\varsigma} = \int_{\Omega} \left(\mathbf{B}_{\varsigma T}^T \hat{\mathbf{D}}_{\varsigma} \mathbf{B}_{\varsigma} + 2\mathbf{B}_{\varsigma T}^T \hat{\mathbf{D}}_{\varsigma} \mathbf{B}_{\varsigma nl} + \mathbf{B}_{\varsigma nl}^T \hat{\mathbf{D}}_{\varsigma} \mathbf{B}_{\varsigma} + 2\mathbf{B}_{\varsigma nl}^T \hat{\mathbf{D}}_{\varsigma} \mathbf{B}_{\varsigma nl} + 2\mathbf{B}_g^T \hat{\mathbf{N}}_{\varsigma} \mathbf{B}_{g\varsigma} \right) d\Omega \tag{23b}$$

$$\mathbf{K}_{T\eta} = \int_{\Omega} \left(\mathbf{B}_{\eta T}^T \mathbf{\Gamma}_{\eta} \hat{\mathbf{D}}_{\eta} \mathbf{B}_{\eta} + 2\mathbf{B}_{\eta T}^T \mathbf{\Gamma}_{\eta} \hat{\mathbf{D}}_{\eta} \mathbf{B}_{\eta nl} + \mathbf{B}_{\eta nl}^T \mathbf{\Gamma}_{\eta} \hat{\mathbf{D}}_{\eta} \mathbf{B}_{\eta} + 2\mathbf{B}_{\eta nl}^T \mathbf{\Gamma}_{\eta} \hat{\mathbf{D}}_{\eta} \mathbf{B}_{\eta nl} + 2\mathbf{B}_g^T \hat{\mathbf{N}}_{\eta} \mathbf{B}_{g\eta} \right) d\Omega \tag{23c}$$

6. Numerical examples

In this section, verification studies and parametric investigations on the post-buckling behavior of FG microplates under mechanical and thermal loads are conducted. For analysis of micro structures, the length scale parameters should be defined based on experimental information. However, the values of length scale parameters of FGMs are not available in the literature. For simplification purpose, the length scale parameters in this study are assumed to be identical $l_0 = l_1 = l_2 = l = 15 \times 10^{-6}$ m [25, 56]. Material properties of FGMs which can be either temperature-independent

or temperature-dependent, and the data is presented in Tables 1 and 2, respectively. The boundary conditions employed in this study are given as described next.

In the case of mechanical loads:

- SSSS1$_m$

$$\theta_x = w = 0 \text{ at } y = 0 \text{ and } y = b \tag{24a}$$

$$\theta_y = w = 0 \text{ at } x = 0 \text{ and } x = a \tag{24b}$$

- SSSS2$_m$

$$u = \theta_x = w = 0 \text{ at } y = 0 \text{ and } y = b \tag{25a}$$

$$v = \theta_y = w = 0 \text{ at } x = 0 \text{ and } x = a \tag{25b}$$

- SCSC$_m$

$$\theta_x = w = 0 \text{ at } y = 0 \text{ and } y = b \tag{26a}$$

$$v = \theta_x = \theta_y = w = \frac{\partial w}{\partial x} = 0 \text{ at } x = 0 \text{ and } x = a \tag{26b}$$

In the case of thermal loads:

- SSSS1$_t$

$$u = \theta_x = w = 0 \text{ at } y = 0 \text{ and } y = b \tag{27a}$$

$$v = \theta_y = w = 0 \text{ at } x = 0 \text{ and } x = a \tag{27b}$$

- SSSS2$_t$

$$u = v = \theta_x = w = 0 \text{ at } y = 0 \text{ and } y = b \tag{28a}$$

$$u = v = \theta_y = w = 0 \text{ at } x = 0 \text{ and } x = a \tag{28b}$$

- CCCC$_t$

$$u = v = \theta_x = \theta_y = w = \frac{\partial w}{\partial y} = 0 \text{ at } y = 0 \text{ and } y = b \tag{29a}$$

$$u = v = \theta_x = \theta_y = w = \frac{\partial w}{\partial x} = 0 \text{ at } x = 0 \text{ and } x = a \tag{29b}$$

In the IGA technique, the conditions related to first derivative of w is treated by setting zero value for the transverse displacement in all control points on the boundary and those adjacent to them. Herein, the choice for boundary conditions in cases of mechanical and thermal loads are different due to the distinctions between the actions of these effects. While the mechanical buckling loads are applied on the edges of the plate and they tend to move all the points in the boundary in their directions, the thermal buckling loads are generated in side the plate domain due to the elevated temperature and the bending-stretching effect.

6.1. Verification studies

Since the results for the post-buckling of FG microplates based on the MST are not available in the literature, the present approach is verified by solving some problems of macro-plates in the literature.

In the first verification, the post-buckling response of an isotropic plate subjected to uniaxial compressive load is addressed. The non-dimensional geometry and material properties are listed as follows: $a = b = 10$, $h = 0.2$, $E = 3 \times 10^6$ and $\nu = 0.25$, and the boundary condition used is SSSS1$_m$. In Fig. 2, the post-buckling paths obtained from Le-Manh and Lee [72] and the present study with different mesh sizes are depicted. Herein, $\lambda = Na^2/\pi^2\bar{D}$ with $\bar{D} = Eh^3/12\left(1-\nu^2\right)$. By adopting cubic basis functions, the solutions obtained from present approach converge quickly and agree well with those given in [72] with 8×8 mesh. Therefore, this mesh size is used in the remaining calculations.

The next verification example examines the post-buckling behavior of FG plates under thermal loads. In Fig. 3, the thermal post-buckling paths of a square SSSS2$_t$ Al2O3/Al plate under nonlinear temperature rise are compared with those given by Tran et al. [16]. The material properties used in this example are assumed to be temperature-independent. As expected, the present results and those obtained from [16] are in good agreement. Another example about the thermal post-buckling response of FG plate is depicted in Fig. 4 for a SSSS2$_t$ Si3N4/SUS304 plate under uniform temperature rise with the material properties being temperature-dependent. The plate in this case has a planar dimension of $a = b = 0.3$ m and $a/h = 100$. It can be seen that the present results are in excellent agreement with those obtained by Park and Kim [7] for different values of gradient index n.

6.2. Parametric studies

In this subsection, parametric studies are conducted to investigate the influences of different parameters, such as material gradient indices, length scale parameters, thickness ratios and boundary conditions, on the post buckling behavior of FG microplates. In case of micoplates subjected to mechanical loadings, the adopted materials are Al2O3/Al. For thermal problems, materials of the plates are Si3N4/SUS304 and temperature-dependent. It should be noted that the temperature change is not usually uniform in the FG plate since the temperature rises much faster at the ceramic part than the metal one. Therefore, only nonlinear temperature rise is considered in the current investigation.

6.2.1. Post-buckling responses under compressive loads

Fig. 5 illustrates the influence of the gradient index n on the post-buckling behavior of FG microplates, in which $\tilde{N} = Na^2/E_m h^3$. The bifurcation buckling is captured in case of isotropic plates

(n = 0 or $n = \infty$) as expected. Whereas, sudden deformations are obtained when the compressive force is applied in case of FG plates. This is due to the coupling moments induced by the difference between the middle and physical neutral surfaces. In general, the buckling load is reduced with the increase of gradient index n. It can be explained that this change gives rise to the metal phrase, which makes the plate become softer.

The influence of size effect on the post-buckling response of FG microplates is depicted in Fig. 6. In general, the bifurcation buckling does not occur in case of FG plates with simply supported (SSSS1$_m$) boundary condition. In addition, it can be seen that the load-carrying capacity increases with the decrease of the ratio of h/l. Herein, $h/l = \infty$ denotes the classical case where the size effect is neglected. When the ratio of h/l decreases, the influence of the size effect becomes more considerable as indicated in the Fig. 6 and become extraordinary when h/l approaches to unity and smaller than unity. In other words, the size effect becomes dominant and the stiffness of the plate increases remarkably when the sizes of the plate is at the microscale.

In Fig. 7, the influence of shear deformation effect on the post-buckling response is illustrated. The behavior of thin plates ($a/h = 100$ and $a/h = 50$) are almost identical since the influence of shear deformation effect is not significant. However, when the thicker plates are considered, the effect becomes noticeable as seen in the Fig. 7.

In the last example, the influence of boundary conditions on the post-buckling response are studied and the results are presented in Fig. 8. In general, the SSSS1$_m$ boundary condition is the weakest (i.e., less stiff) case in post-buckling analysis, followed by the SSSS2$_m$ and SCSC$_m$ boundary conditions. This observation can be explained by the fact that the SSSS1$_m$ boundary condition imposes less geometric constraints than other cases, whose in-plane displacements at the edges are fixed. Furthermore, it is noticed that the clamped boundary condition is capable of preventing the plate from sudden deformations, although the plate in this case is made from FGMs with coupling moments being generated. It should be noted that the uniaxial compressive forces are imposed in the clamped edges in this investigation.

6.2.2. Post-buckling responses under nonlinear temperature rise

The influence of gradient index n on the thermal response is presented in Fig. 9. As can be seen from the figure, the plate deforms immediately when the temperature at the upper surface is raised regardless of isotropic materials ($n = 0$ or $n = \infty$) or FGMs. This is due to the nonlinear temperature variation, which leads to the generation of thermal moments $\mathbf{M}_T^{\varepsilon}$ and high-order thermal stress resultants $\mathbf{L}_T^{\varepsilon}$ as given in Eq. (14). In addition, it is worth noting that the variation of thermal post-buckling path with respect to the gradient index n does not follow a monotonic manner. Compared

to the purely ceramic case, higher temperature resistance is obtained when the gradient index n is prescribed as $n = 1$ or 2. However, the thermal post-buckling paths of other cases with $n \geq 5$ are lower compared to that with $n = 0$. This is due to the fact that the temperature field nonlinearly varies throughout the plate thickness, and the temperature distribution profile varies with different gradient indices. Similar observation was also reported in the study of Ma and Wang [4]. In addition, it should be noted that the plate in this example deforms to the upper side. Herein, the higher temperatures are applied to the ceramic surface and the temperature at the bottom is keep constant at 300^0K. This condition makes the top of the plate expands more than the bottom side does. Consequently, upward deflections are obtained. In the case of uniform temperature rise discussed in the verification studies, the FG plate bends downward since the material at the bottom surface has a larger value of thermal expansion coefficient.

In Fig. 10, the influence of size effect on the thermal post-buckling behaviour of FG microplates is illustrated. The obtained results show that the thermal behaviour of FG microplates is remarkably affected by the size effect. When the influence of size effect is relatively small (h/l = 10 to h/l = 5), the thermal post-buckling path slightly increases compared to the classical case (h/l = ∞). However, when the size effect becomes most considerable (h/l = 2 to h/l = 0.5), the shapes of post-buckling paths change completely. In these case, the microplate becomes much stiffer and its thermal resistance is extraordinarily raised.

The influence of thickness ratio on the thermal post-buckling behavior of FG microplates is depicted in Fig. 11. In general, when the plates are changed from thin to thick, their behavior at different thickness ratios are completely different to each others. It is seen that the thinner the plate is, the more unstably it behaves under the thermal loadings. When the plate becomes thicker, its thermal resistance increases considerably. Unlike the case of microplates subjected to mechanical loadings, the influence of thickness ratio on the thermal post-buckling responses is more significant. Herein, the thickness ratio not only influences on the impact of shear deformation effect but also affects the temperature variation throughout the plate thickness as defined in Eq. (3). Therefore, shear deformation theory should be taken into consideration to accurately predict the behavior of FG plates under thermal loadings.

The final example is contributed to the investigation of the influence of three types of boundary conditions, namely SSSS1$_t$, SSSS2$_t$ and CCCC$_t$, on the thermal post-buckling behavior of FG microplates. As can be seen in Fig. 12, the bifurcation buckling is captured in the case of clamped boundary condition (CCCC$_t$), even though the problem considered herein is carried out with the nonlinear temperature rise. In other cases, where the simply supported boundary conditions are ex-

amined, the plate buckles as soon as the temperature rise is considered. In addition, the clamped boundary condition is seen to have a considerable impact on the thermal resistance of the plate. The buckling temperature in such case is much higher than other cases of simply supported boundary conditions. Furthermore, it is seen that the plate with movable edges (SSSS1_t) produces smaller displacements than that with immovable edges (SSSS2_t). This observation is inverse to that in the previous study on the post-buckling of microplates under mechanical loads. Herein, the adoption of movable boundary condition makes the plate free to expand, whereas the immovable one restrains the expansion of the plate via its edges, and consequently lager deflections are obtained.

7. Conclusions

In this study, a numerical approach based on the IGA is developed to study the post-buckling behavior of FG microplates under mechanical and thermal loads. The size effect inherited from the micro-structure is accounted for using the MST, whilst the shear deformation effect and geometric nonlinearity are captured using the Reddy third-order shear deformation theory along with the von Kámán's assumption. The material variations throughout the plate thickness are described using the rule of mixtures, and temperature-dependent materials are also taken into consideration. The principle of virtual work is used to derived the governing equations, which are then discretized using the IGA approach. The interpolation functions with C^2-continuity are obtained naturally and efficiently. The Newton's iterative technique with imperfection is employed to solve the nonlinear equations. Some verification problems are solved to prove the accuracy of the present approach. Parametric studies are also conducted to examine the influences of the value of the gradient index, size effect, thickness ratios, and boundary conditions. The following specific conclusions are drawn from the present study:

- Larger post-buckling deformations under compressive loads are obtained when the gradient index is increased (because larger values correspond to lower modulus). For thermal post-buckling problems, the influence of the gradient index is noticeable as it is found that the thermal resistance of the plate in some cases is greater than that of purely ceramic plate.

- The size effect (material length scale) has a remarkable influence on the post-buckling behavior of microplates. When the plate thickness is comparable to the length scale parameter, the size effect becomes most significant, consequently the post-buckling deformation is much smaller than that obtained from the classical theory.

- The effect of thickness ratios on thermal post-buckling response is noticeable as it influences not only the shear deformation effect but also the temperature distribution through the thickness.

- The FG plates with simply supported boundary conditions are unstable under the effect of both compressive and thermal loads, whereas the clamped boundary condition is capable of preventing the plates from sudden deformations, and the bifurcation buckling is obtained consequently.

Acknowledgements

This research study was supported by a Postgraduate Research Scholarship at La Trobe University. This financial support is gratefully acknowledged.

Appendix A

The components of strain-displacement vectors are given as follows

$$\boldsymbol{\varepsilon}=\left\{\begin{array}{c}\varepsilon_{xx}\\ \varepsilon_{yy}\\ \gamma_{xy}\end{array}\right\};\ \boldsymbol{\varepsilon}_0=\left\{\begin{array}{c}u_{,x}\\ v_{,y}\\ u_{,y}+v_{,x}\end{array}\right\};\boldsymbol{\varepsilon}_{nl}=\left\{\begin{array}{c}(w_{,x})^2\\ (w_{,y})^2\\ 2w_{,x}w_{,y}\end{array}\right\};\boldsymbol{\varepsilon}_1=\left\{\begin{array}{c}\theta_{x,x}\\ \theta_{y,y}\\ \theta_{x,y}+\theta_{y,x}\end{array}\right\};\boldsymbol{\varepsilon}_2=\left\{\begin{array}{c}-w_{,xx}\\ -w_{,yy}\\ -2w_{,xy}\end{array}\right\} \tag{A-1a}$$

$$\boldsymbol{\gamma}=\left\{\begin{array}{c}\gamma_{xz}\\ \gamma_{yz}\end{array}\right\};\ \boldsymbol{\gamma}_1=\left\{\begin{array}{c}\theta_x\\ \theta_y\end{array}\right\};\boldsymbol{\gamma}_2=\left\{\begin{array}{c}w_{,x}\\ w_{,y}\end{array}\right\} \tag{A-1b}$$

$$\boldsymbol{\varsigma}=\left\{\begin{array}{c}\varsigma_x\\ \varsigma_y\end{array}\right\};\boldsymbol{\varsigma}_0=\left\{\begin{array}{c}u_{,xx}+v_{,xy}\\ u_{,xy}+v_{,yy}\end{array}\right\};\boldsymbol{\varsigma}_{nl}=\left\{\begin{array}{c}w_{,x}w_{,xx}+w_{,y}w_{,xy}\\ w_{,x}w_{,xy}+w_{,y}w_{,yy}\end{array}\right\} \tag{A-2a}$$

$$\boldsymbol{\varsigma}_1=\left\{\begin{array}{c}\theta_{x,xx}+\theta_{y,xy}\\ \theta_{x,xy}+\theta_{y,yy}\end{array}\right\};\boldsymbol{\varsigma}_2=\left\{\begin{array}{c}-w_{,xxx}-w_{,xyy}\\ -w_{,xxy}-w_{,yyy}\end{array}\right\} \tag{A-2b}$$

$$\varsigma_3=\theta_{x,x}+\theta_{y,y};\varsigma_4=-w_{,xx}-w_{,yy} \tag{A-2c}$$

$$\boldsymbol{\eta}=\left\{\begin{array}{c}\eta^{(1)}_{xxx}\\ \eta^{(1)}_{yyy}\\ \eta^{(1)}_{zzz}\\ \eta^{(1)}_{xxy}\\ \eta^{(1)}_{xxz}\\ \eta^{(1)}_{xyy}\\ \eta^{(1)}_{xyz}\\ \eta^{(1)}_{xzz}\\ \eta^{(1)}_{yyz}\\ \eta^{(1)}_{yzz}\end{array}\right\};\boldsymbol{\eta}_0=\left\{\begin{array}{c}\frac{2}{5}u_{,xx}-\frac{1}{5}u_{,yy}-\frac{2}{5}v_{,xy}\\ -\frac{2}{5}u_{,xy}+\frac{2}{5}v_{,yy}-\frac{1}{5}v_{,xx}\\ -\frac{1}{5}w_{,xx}-\frac{1}{5}w_{,yy}\\ \frac{8}{15}u_{,xy}+\frac{4}{15}v_{,xx}-\frac{1}{5}v_{,yy}\\ \frac{4}{15}w_{,xx}-\frac{1}{15}w_{,yy}\\ \frac{4}{15}u_{,yy}-\frac{1}{5}u_{,xx}+\frac{8}{15}v_{,xy}\\ \frac{1}{3}w_{,xy}\\ -\frac{1}{5}u_{,xx}-\frac{1}{15}u_{,yy}-\frac{2}{15}v_{,xy}\\ \frac{4}{15}w_{,yy}-\frac{1}{15}w_{,xx}\\ -\frac{2}{15}u_{,xy}-\frac{1}{15}v_{,xx}-\frac{1}{5}v_{,yy}\end{array}\right\};\boldsymbol{\eta}_{nl}=\left\{\begin{array}{c}\frac{2}{5}w_{,x}w_{,xx}-\frac{1}{5}w_{,x}w_{,yy}-\frac{2}{5}w_{,y}w_{,xy}\\ -\frac{2}{5}w_{,x}w_{,xy}-\frac{1}{5}w_{,y}w_{,xx}+\frac{2}{5}w_{,y}w_{,yy}\\ 0\\ \frac{8}{15}w_{,x}w_{,xy}+\frac{4}{15}w_{,y}w_{,xx}-\frac{1}{5}w_{,y}w_{,yy}\\ 0\\ -\frac{1}{5}w_{,x}w_{,xx}+\frac{4}{15}w_{,x}w_{,yy}+\frac{8}{15}w_{,y}w_{,xy}\\ 0\\ -\frac{1}{5}w_{,x}w_{,xx}-\frac{1}{15}w_{,x}w_{,yy}-\frac{2}{15}w_{,y}w_{,xy}\\ 0\\ -\frac{2}{15}w_{,x}w_{,xy}-\frac{1}{15}w_{,y}w_{,xx}-\frac{1}{5}w_{,y}w_{,yy}\end{array}\right\} \tag{A-3a}$$

$$\boldsymbol{\eta}_1 = \begin{Bmatrix} -\frac{1}{5}\theta_x \\ -\frac{1}{5}\theta_y \\ 0 \\ -\frac{1}{15}\theta_y \\ 0 \\ -\frac{1}{15}\theta_x \\ 0 \\ \frac{4}{15}\theta_x \\ 0 \\ \frac{4}{15}\theta_y \end{Bmatrix}; \boldsymbol{\eta}_2 = \begin{Bmatrix} 0 \\ 0 \\ -\frac{2}{5}\theta_{x,x} - \frac{2}{5}\theta_{y,y} \\ 0 \\ \frac{8}{15}\theta_{x,x} - \frac{2}{15}\theta_{y,y} \\ 0 \\ \frac{1}{3}\theta_{x,y} + \frac{1}{3}\theta_{y,x} \\ 0 \\ -\frac{2}{15}\theta_{x,x} + \frac{8}{15}\theta_{y,y} \\ 0 \end{Bmatrix}; \boldsymbol{\eta}_3 = \begin{Bmatrix} \frac{2}{5}\theta_{x,xx} - \frac{1}{5}\theta_{x,yy} - \frac{2}{5}\theta_{y,xy} \\ -\frac{2}{5}\theta_{x,xy} - \frac{1}{5}\theta_{y,xx} + \frac{2}{5}\theta_{y,yy} \\ 0 \\ \frac{8}{15}\theta_{x,xy} + \frac{4}{15}\theta_{y,xx} - \frac{1}{5}\theta_{y,yy} \\ 0 \\ -\frac{1}{5}\theta_{x,xx} + \frac{4}{15}\theta_{x,yy} + \frac{8}{15}\theta_{y,xy} \\ 0 \\ -\frac{1}{5}\theta_{x,xx} - \frac{1}{15}\theta_{x,yy} - \frac{2}{15}\theta_{y,xy} \\ 0 \\ -\frac{2}{15}\theta_{x,xy} - \frac{1}{15}\theta_{y,xx} - \frac{1}{5}\theta_{y,yy} \end{Bmatrix} \tag{A-3b}$$

$$\boldsymbol{\eta}_4 = \begin{Bmatrix} \frac{1}{5}w_{,x} \\ \frac{1}{5}w_{,y} \\ 0 \\ \frac{1}{15}w_{,y} \\ 0 \\ \frac{1}{15}w_{,x} \\ 0 \\ -\frac{4}{15}w_{,x} \\ 0 \\ -\frac{4}{15}w_{,y} \end{Bmatrix}; \boldsymbol{\eta}_5 = \begin{Bmatrix} 0 \\ 0 \\ \frac{2}{5}w_{,xx} + \frac{2}{5}w_{,yy} \\ 0 \\ -\frac{8}{15}w_{,xx} + \frac{2}{15}w_{,yy} \\ 0 \\ -\frac{1}{2}w_{,xy} \\ 0 \\ \frac{2}{15}w_{,xx} - \frac{8}{15}w_{,yy} \\ 0 \end{Bmatrix}; \boldsymbol{\eta}_6 = \begin{Bmatrix} -\frac{2}{5}w_{,xxx} + \frac{3}{5}w_{,xyy} \\ -\frac{2}{5}w_{,yyy} + \frac{3}{5}w_{,xxy} \\ 0 \\ -\frac{4}{5}w_{,xxy} + \frac{1}{5}w_{,yyy} \\ 0 \\ \frac{1}{5}w_{,xxx} - \frac{4}{5}w_{,xyy} \\ 0 \\ \frac{1}{5}w_{,xxx} + \frac{1}{5}w_{,xyy} \\ 0 \\ \frac{1}{5}w_{,xxy} + \frac{1}{5}w_{,yyy} \end{Bmatrix} \tag{A-3c}$$

$$\boldsymbol{\chi} = \begin{Bmatrix} \chi^s_{xx} \\ \chi^s_{yy} \\ \chi^s_{xy} \\ \chi^s_{zz} \\ \chi^s_{xz} \\ \chi^s_{yz} \end{Bmatrix}; \boldsymbol{\chi}_0 = \begin{Bmatrix} \frac{1}{2}w_{,xy} \\ -\frac{1}{2}w_{,xy} \\ \frac{1}{4}w_{,yy} - \frac{1}{4}w_{,xx} \\ 0 \\ -\frac{1}{4}u_{,xy} + \frac{1}{4}v_{,xx} \\ -\frac{1}{4}u_{,yy} + \frac{1}{4}v_{,xy} \end{Bmatrix}; \boldsymbol{\chi}_1 = \begin{Bmatrix} 0 \\ 0 \\ 0 \\ 0 \\ -\frac{1}{4}\theta_y \\ \frac{1}{4}\theta_x \end{Bmatrix}; \boldsymbol{\chi}_2 = \begin{Bmatrix} -\frac{1}{2}\theta_{y,x} \\ \frac{1}{2}\theta_{x,y} \\ \frac{1}{4}\theta_{x,x} - \frac{1}{4}\theta_{y,y} \\ -\frac{1}{2}\theta_{x,y} + \frac{1}{2}\theta_{y,x} \\ 0 \\ 0 \end{Bmatrix} \tag{A-4a}$$

$$\boldsymbol{\chi}_3 = \begin{Bmatrix} 0 \\ 0 \\ 0 \\ 0 \\ -\frac{1}{4}\theta_{x,xy} + \frac{1}{4}\theta_{y,xx} \\ -\frac{1}{4}\theta_{x,yy} + \frac{1}{4}\theta_{y,xy} \end{Bmatrix}; \boldsymbol{\chi}_4 = \begin{Bmatrix} 0 \\ 0 \\ 0 \\ 0 \\ \frac{1}{4}w_{,y} \\ -\frac{1}{4}w_{,x} \end{Bmatrix}; \boldsymbol{\chi}_5 = \begin{Bmatrix} \frac{1}{2}w_{,xy} \\ -\frac{1}{2}w_{,xy} \\ \frac{1}{4}w_{,yy} - \frac{1}{4}w_{,xx} \\ 0 \\ 0 \\ 0 \end{Bmatrix} \tag{A-4b}$$

Appendix B

The definitions of constituent matrices $\hat{\mathbf{D}}_{\varepsilon}, \hat{\mathbf{D}}_{\varsigma}, \hat{\mathbf{D}}_{\eta}, \hat{\mathbf{D}}_{\chi}$ are given as follows

$$\hat{\mathbf{D}}_{\varepsilon} = \int_{-h/2}^{h/2} \begin{Bmatrix} 1 \\ f(z) \\ g(z) \\ \mathbf{0} \\ \mathbf{0} \end{Bmatrix} \begin{Bmatrix} \mathbf{Q}_b \\ f(z)\mathbf{Q}_b \\ g(z)\mathbf{Q}_b \\ \mathbf{0} \\ \mathbf{0} \end{Bmatrix}^T dz + \int_{-h/2}^{h/2} \begin{Bmatrix} \mathbf{0} \\ \mathbf{0} \\ \mathbf{0} \\ f'(z) \\ 1-g'(z) \end{Bmatrix} \begin{Bmatrix} \mathbf{0} \\ \mathbf{0} \\ \mathbf{0} \\ f'(z)\mathbf{Q}_s \\ [1-g'(z)]\mathbf{Q}_s \end{Bmatrix}^T dz \quad \text{(B-1a)}$$

$$\hat{\mathbf{D}}_{\varsigma} = \int_{-h/2}^{h/2} 2\mu l_0^2 \begin{Bmatrix} 1 \\ f(z) \\ g(z) \\ 0 \\ 0 \end{Bmatrix} \begin{Bmatrix} 1 \\ f(z) \\ g(z) \\ 0 \\ 0 \end{Bmatrix}^T dz + \int_{-h/2}^{h/2} 2\mu l_0^2 \begin{Bmatrix} 0 \\ 0 \\ 0 \\ f'(z) \\ g'(z) \end{Bmatrix} \begin{Bmatrix} 0 \\ 0 \\ 0 \\ f'(z) \\ g'(z) \end{Bmatrix}^T dz \quad \text{(B-1b)}$$

$$\hat{\mathbf{D}}_{\eta} = \int_{-h/2}^{h/2} 2\mu l_1^2 \begin{Bmatrix} 1 \\ f''(z) \\ f'(z) \\ f(z) \\ g''(z) \\ g'(z) \\ g(z) \end{Bmatrix} \begin{Bmatrix} 1 \\ f''(z) \\ f'(z) \\ f(z) \\ g''(z) \\ g'(z) \\ g(z) \end{Bmatrix}^T dz \quad \text{(B-1c)}$$

$$\hat{\mathbf{D}}_{\chi} = \int_{-h/2}^{h/2} 2\mu l_2^2 \begin{Bmatrix} 1 \\ f''(z) \\ f'(z) \\ f(z) \\ g''(z) \\ g'(z) \end{Bmatrix} \begin{Bmatrix} 1 \\ f''(z) \\ f'(z) \\ f(z) \\ g''(z) \\ g'(z) \end{Bmatrix}^T dz \quad \text{(B-1d)}$$

where

$$\mathbf{Q}_b = \frac{E(z)}{1-\nu^2(z)} \begin{bmatrix} 1 & \nu(z) & 0 \\ \nu(z) & 1 & 0 \\ 0 & 0 & (1-\nu(z))/2 \end{bmatrix}; \ \mathbf{Q}_s = \frac{E(z)}{2(1+\nu(z))} \begin{bmatrix} 1 & 0 \\ 0 & 1 \end{bmatrix} \quad \text{(B-2)}$$

Appendix C

Details of strain-displacement matrices are expressed as followed

$$\mathbf{B}_{\varepsilon}=\left\{\begin{array}{c}\mathbf{B}_{\varepsilon}^{0}\\ \mathbf{B}_{\varepsilon}^{1}\\ \mathbf{B}_{\varepsilon}^{2}\\ \mathbf{B}_{\varepsilon}^{3}\\ \mathbf{B}_{\varepsilon}^{4}\end{array}\right\};\mathbf{B}_{\varepsilon T}=\left\{\begin{array}{c}\left(\mathbf{B}_{\varepsilon}^{0}\right)^{T}\\ \left(\mathbf{B}_{\varepsilon}^{1}\right)^{T}\\ \left(\mathbf{B}_{\varepsilon}^{2}\right)^{T}\\ \left(\mathbf{B}_{\varepsilon}^{3}\right)^{T}\\ \left(\mathbf{B}_{\varepsilon}^{4}\right)^{T}\end{array}\right\};\mathbf{B}_{\varsigma}=\left\{\begin{array}{c}\mathbf{B}_{\varsigma}^{0}\\ \mathbf{B}_{\varsigma}^{1}\\ \mathbf{B}_{\varsigma}^{2}\\ \mathbf{B}_{\varsigma}^{3}\\ \mathbf{B}_{\varsigma}^{4}\end{array}\right\};\mathbf{B}_{\varsigma T}=\left\{\begin{array}{c}\left(\mathbf{B}_{\varsigma}^{0}\right)^{T}\\ \left(\mathbf{B}_{\varsigma}^{1}\right)^{T}\\ \left(\mathbf{B}_{\varsigma}^{2}\right)^{T}\\ \left(\mathbf{B}_{\varsigma}^{3}\right)^{T}\\ \left(\mathbf{B}_{\varsigma}^{4}\right)^{T}\end{array}\right\} \tag{C-1a}$$

$$\mathbf{B}_{\eta}=\left\{\begin{array}{c}\mathbf{B}_{\eta}^{0}\\ \mathbf{B}_{\eta}^{1}\\ \mathbf{B}_{\eta}^{2}\\ \mathbf{B}_{\eta}^{3}\\ \mathbf{B}_{\eta}^{4}\\ \mathbf{B}_{\eta}^{5}\\ \mathbf{B}_{\eta}^{6}\end{array}\right\};\mathbf{B}_{\eta T}=\left\{\begin{array}{c}\left(\mathbf{B}_{\eta}^{0}\right)^{T}\\ \left(\mathbf{B}_{\eta}^{1}\right)^{T}\\ \left(\mathbf{B}_{\eta}^{2}\right)^{T}\\ \left(\mathbf{B}_{\eta}^{3}\right)^{T}\\ \left(\mathbf{B}_{\eta}^{4}\right)^{T}\\ \left(\mathbf{B}_{\eta}^{5}\right)^{T}\\ \left(\mathbf{B}_{\eta}^{6}\right)^{T}\end{array}\right\};\mathbf{B}_{\chi}=\left\{\begin{array}{c}\mathbf{B}_{\chi}^{0}\\ \mathbf{B}_{\chi}^{1}\\ \mathbf{B}_{\chi}^{2}\\ \mathbf{B}_{\chi}^{3}\\ \mathbf{B}_{\chi}^{4}\\ \mathbf{B}_{\chi}^{5}\end{array}\right\}\mathbf{B}_{\chi T}=\left\{\begin{array}{c}\left(\mathbf{B}_{\chi}^{0}\right)^{T}\\ \left(\mathbf{B}_{\chi}^{1}\right)^{T}\\ \left(\mathbf{B}_{\chi}^{2}\right)^{T}\\ \left(\mathbf{B}_{\chi}^{3}\right)^{T}\\ \left(\mathbf{B}_{\chi}^{4}\right)^{T}\\ \left(\mathbf{B}_{\chi}^{5}\right)^{T}\end{array}\right\} \tag{C-1b}$$

where

$$\mathbf{B}_{\varepsilon c}^{0}=\begin{bmatrix}R_{c,x} & 0 & 0 & 0 & 0\\ 0 & R_{c,y} & 0 & 0 & 0\\ R_{c,y} & R_{c,x} & 0 & 0 & 0\end{bmatrix};\mathbf{B}_{\varepsilon c}^{1}=\begin{bmatrix}0 & 0 & R_{c,x} & 0 & 0\\ 0 & 0 & 0 & R_{c,y} & 0\\ 0 & 0 & R_{c,y} & R_{c,x} & 0\end{bmatrix} \tag{C-2a}$$

$$\mathbf{B}_{\varepsilon c}^{2}=\begin{bmatrix}0 & 0 & 0 & 0 & -R_{c,xx}\\ 0 & 0 & 0 & 0 & -R_{c,yy}\\ 0 & 0 & 0 & 0 & -2R_{c,xy}\end{bmatrix};\mathbf{B}_{\varepsilon c}^{3}=\begin{bmatrix}0 & 0 & R_{c} & 0 & 0\\ 0 & 0 & 0 & R_{c} & 0\end{bmatrix} \tag{C-2b}$$

$$\mathbf{B}_{\varepsilon c}^{4}=\begin{bmatrix}0 & 0 & 0 & 0 & R_{c,x}\\ 0 & 0 & 0 & 0 & R_{c,y}\end{bmatrix} \tag{C-2c}$$

$$\mathbf{B}_{\varsigma}^{0}=\begin{bmatrix}R_{c,xx} & R_{c,xy} & 0 & 0 & 0\\ R_{c,xy} & R_{c,yy} & 0 & 0 & 0\end{bmatrix};\mathbf{B}_{\varsigma}^{1}=\begin{bmatrix}0 & R_{c,xx} & R_{c,xy} & 0 & 0\\ 0 & R_{c,xy} & R_{c,yy} & 0 & 0\end{bmatrix} \tag{C-3a}$$

$$\mathbf{B}_{\varsigma}^{2}=\begin{bmatrix}0 & 0 & 0 & 0 & -R_{c,xxx}-R_{c,xyy}\\ 0 & 0 & 0 & 0 & -R_{c,xxy}-R_{c,yyy}\end{bmatrix};\mathbf{B}_{\varsigma c}^{3}=\begin{bmatrix}0 & 0 & R_{c,x} & R_{c,y} & 0\end{bmatrix} \tag{C-3b}$$

$$\mathbf{B}_{\varsigma c}^{4}=\begin{bmatrix}0 & 0 & 0 & 0 & -R_{c,xx}-R_{c,yy}\end{bmatrix} \tag{C-3c}$$

$$\mathbf{B}^0_{\eta c} = \begin{bmatrix} \frac{2}{5}R_{c,xx} - \frac{1}{5}R_{c,yy} & -\frac{2}{5}R_{c,xy} & 0 & 0 & 0 \\ -\frac{2}{5}R_{c,xy} & \frac{2}{5}R_{c,yy} - \frac{1}{5}R_{c,xx} & 0 & 0 & 0 \\ 0 & 0 & 0 & 0 & -\frac{1}{5}R_{c,xx} - \frac{1}{5}R_{c,yy} \\ \frac{8}{15}R_{c,xy} & \frac{4}{15}R_{c,xx} - \frac{1}{5}R_{c,yy} & 0 & 0 & 0 \\ 0 & 0 & 0 & 0 & \frac{4}{15}R_{c,xx} - \frac{1}{15}R_{c,yy} \\ \frac{4}{15}R_{c,yy} - \frac{1}{5}R_{c,xx} & \frac{8}{15}R_{c,xy} & 0 & 0 & 0 \\ 0 & 0 & 0 & 0 & \frac{1}{3}R_{c,xy} \\ -\frac{1}{5}R_{c,xx} - \frac{1}{15}R_{c,yy} & -\frac{2}{15}R_{c,xy} & 0 & 0 & 0 \\ 0 & 0 & 0 & 0 & -\frac{1}{15}R_{c,xx} + \frac{4}{15}R_{c,yy} \\ -\frac{2}{15}R_{c,xy} & -\frac{1}{15}R_{c,xx} - \frac{1}{5}R_{c,yy} & 0 & 0 & 0 \end{bmatrix} \tag{C-4a}$$

$$\mathbf{B}^1_{\eta c} = \begin{bmatrix} 0 & 0 & -\frac{1}{5}R_c & 0 & 0 \\ 0 & 0 & 0 & -\frac{1}{5}R_c & 0 \\ 0 & 0 & 0 & 0 & 0 \\ 0 & 0 & 0 & -\frac{1}{15}R_c & 0 \\ 0 & 0 & 0 & 0 & 0 \\ 0 & 0 & -\frac{1}{15}R_c & 0 & 0 \\ 0 & 0 & 0 & 0 & 0 \\ 0 & 0 & \frac{4}{15}R_c & 0 & 0 \\ 0 & 0 & 0 & 0 & 0 \\ 0 & 0 & 0 & \frac{4}{15}R_c & 0 \end{bmatrix}; \mathbf{B}^2_{\eta} = \begin{bmatrix} 0 & 0 & 0 & 0 & 0 \\ 0 & 0 & 0 & 0 & 0 \\ 0 & 0 & -\frac{2}{5}R_{c,x} & -\frac{2}{5}R_{c,y} & 0 \\ 0 & 0 & 0 & 0 & 0 \\ 0 & 0 & \frac{8}{15}R_{c,x} & -\frac{2}{15}R_{c,y} & 0 \\ 0 & 0 & 0 & 0 & 0 \\ 0 & 0 & \frac{1}{3}R_{c,y} & \frac{1}{3}R_{c,x} & 0 \\ 0 & 0 & 0 & 0 & 0 \\ 0 & 0 & -\frac{2}{15}R_{c,x} & \frac{8}{15}R_{c,y} & 0 \\ 0 & 0 & 0 & 0 & 0 \end{bmatrix} \tag{C-4b}$$

$$\mathbf{B}^3_{\eta} = \begin{bmatrix} 0 & 0 & \frac{2}{5}R_{c,xx} - \frac{1}{5}R_{c,yy} & -\frac{2}{5}R_{c,xy} & 0 \\ 0 & 0 & -\frac{2}{5}R_{c,xy} & \frac{2}{5}R_{c,yy} - \frac{1}{5}R_{c,xx} & 0 \\ 0 & 0 & 0 & 0 & 0 \\ 0 & 0 & \frac{8}{15}R_{c,xy} & \frac{4}{15}R_{c,xx} - \frac{1}{5}R_{c,yy} & 0 \\ 0 & 0 & 0 & 0 & 0 \\ 0 & 0 & -\frac{1}{5}R_{c,xx} & \frac{4}{15}R_{c,yy} + \frac{8}{15}R_{c,xy} & 0 \\ 0 & 0 & 0 & 0 & 0 \\ 0 & 0 & -\frac{1}{5}R_{c,xx} - \frac{1}{15}R_{c,yy} & -\frac{2}{15}R_{c,xy} & 0 \\ 0 & 0 & 0 & 0 & 0 \\ 0 & 0 & -\frac{2}{15}R_{c,xy} & -\frac{1}{15}R_{c,xx} - \frac{1}{5}R_{c,yy} & 0 \end{bmatrix}; \mathbf{B}^4_{\eta} = \begin{bmatrix} 0 & 0 & 0 & 0 & \frac{1}{5}R_{c,x} \\ 0 & 0 & 0 & 0 & \frac{1}{5}R_{c,y} \\ 0 & 0 & 0 & 0 & 0 \\ 0 & 0 & 0 & 0 & \frac{1}{15}R_{c,y} \\ 0 & 0 & 0 & 0 & 0 \\ 0 & 0 & 0 & 0 & \frac{1}{15}R_{c,x} \\ 0 & 0 & 0 & 0 & 0 \\ 0 & 0 & 0 & 0 & -\frac{4}{15}R_{c,x} \\ 0 & 0 & 0 & 0 & 0 \\ 0 & 0 & 0 & 0 & -\frac{4}{15}R_{c,y} \end{bmatrix} \tag{C-4c}$$

$$\mathbf{B}^5_{\eta c} = \begin{bmatrix} 0 & 0 & 0 & 0 & 0 \\ 0 & 0 & 0 & 0 & 0 \\ 0 & 0 & 0 & 0 & \frac{2}{5}R_{c,xx} + \frac{2}{5}R_{c,yy} \\ 0 & 0 & 0 & 0 & 0 \\ 0 & 0 & 0 & 0 & -\frac{8}{15}R_{c,xx} + \frac{2}{15}R_{c,yy} \\ 0 & 0 & 0 & 0 & 0 \\ 0 & 0 & 0 & 0 & -\frac{1}{2}R_{c,xy} \\ 0 & 0 & 0 & 0 & 0 \\ 0 & 0 & 0 & 0 & \frac{2}{15}R_{c,xx} - \frac{8}{15}R_{c,yy} \\ 0 & 0 & 0 & 0 & 0 \end{bmatrix}; \mathbf{B}^6_{\eta c} = \begin{bmatrix} 0 & 0 & 0 & 0 & -\frac{2}{5}R_{c,xxx} + \frac{3}{5}R_{c,xyy} \\ 0 & 0 & 0 & 0 & -\frac{2}{5}R_{c,yyy} + \frac{3}{5}R_{c,xxy} \\ 0 & 0 & 0 & 0 & 0 \\ 0 & 0 & 0 & 0 & -\frac{4}{5}R_{c,xxy} + \frac{1}{5}R_{c,yyy} \\ 0 & 0 & 0 & 0 & 0 \\ 0 & 0 & 0 & 0 & \frac{1}{5}R_{c,xxx} - \frac{4}{5}R_{c,xyy} \\ 0 & 0 & 0 & 0 & 0 \\ 0 & 0 & 0 & 0 & \frac{1}{5}R_{c,xxx} + \frac{1}{5}R_{c,xyy} \\ 0 & 0 & 0 & 0 & 0 \\ 0 & 0 & 0 & 0 & \frac{1}{5}R_{c,xxy} + \frac{1}{5}R_{c,yyy} \end{bmatrix} \quad \text{(C-4d)}$$

$$\mathbf{B}^0_{\chi} = \begin{bmatrix} 0 & 0 & 0 & 0 & \frac{1}{2}R_{c,xy} \\ 0 & 0 & 0 & 0 & -\frac{1}{2}R_{c,xy} \\ 0 & 0 & 0 & 0 & \frac{1}{4}R_{c,yy} - \frac{1}{4}R_{c,xx} \\ 0 & 0 & 0 & 0 & 0 \\ -\frac{1}{4}R_{c,xy} & \frac{1}{4}R_{c,xx} & 0 & 0 & 0 \\ -\frac{1}{4}R_{c,yy} & \frac{1}{4}R_{c,xy} & 0 & 0 & 0 \end{bmatrix}; \mathbf{B}^1_{\chi} = \begin{bmatrix} 0 & 0 & 0 & 0 & 0 \\ 0 & 0 & 0 & 0 & 0 \\ 0 & 0 & 0 & 0 & 0 \\ 0 & 0 & 0 & 0 & 0 \\ 0 & 0 & 0 & -\frac{1}{4}R_c & 0 \\ 0 & 0 & \frac{1}{4}R_c & 0 & 0 \end{bmatrix} \quad \text{(C-5a)}$$

$$\mathbf{B}^2_{\chi} = \begin{bmatrix} 0 & 0 & 0 & -\frac{1}{2}R_{c,x} & 0 \\ 0 & 0 & \frac{1}{2}R_{c,y} & 0 & 0 \\ 0 & 0 & \frac{1}{4}R_{c,x} & -\frac{1}{4}R_{c,y} & 0 \\ 0 & 0 & -\frac{1}{2}R_{c,y} & \frac{1}{2}R_{c,x} & 0 \\ 0 & 0 & 0 & 0 & 0 \\ 0 & 0 & 0 & 0 & 0 \end{bmatrix}; \mathbf{B}^3_{\chi} = \begin{bmatrix} 0 & 0 & 0 & 0 & 0 \\ 0 & 0 & 0 & 0 & 0 \\ 0 & 0 & 0 & 0 & 0 \\ 0 & 0 & 0 & 0 & 0 \\ 0 & 0 & -\frac{1}{4}R_{c,xy} & \frac{1}{4}R_{c,xx} & 0 \\ 0 & 0 & -\frac{1}{4}R_{c,yy} & \frac{1}{4}R_{c,xy} & 0 \end{bmatrix} \quad \text{(C-5b)}$$

$$\mathbf{B}^4_{\chi c} = \begin{bmatrix} 0 & 0 & 0 & 0 & 0 \\ 0 & 0 & 0 & 0 & 0 \\ 0 & 0 & 0 & 0 & 0 \\ 0 & 0 & 0 & 0 & 0 \\ 0 & 0 & 0 & 0 & \frac{1}{4}R_{c,y} \\ 0 & 0 & 0 & 0 & -\frac{1}{4}R_{c,x} \end{bmatrix}; \mathbf{B}^5_{\chi c} = \begin{bmatrix} 0 & 0 & 0 & 0 & \frac{1}{2}R_{c,xy} \\ 0 & 0 & 0 & 0 & -\frac{1}{2}R_{c,xy} \\ 0 & 0 & 0 & 0 & \frac{1}{4}R_{c,yy} - \frac{1}{4}R_{c,xx} \\ 0 & 0 & 0 & 0 & 0 \\ 0 & 0 & 0 & 0 & 0 \\ 0 & 0 & 0 & 0 & 0 \end{bmatrix} \quad \text{(C-5c)}$$

$$\mathbf{B}_g = \begin{bmatrix} 0 & 0 & 0 & 0 & R_{c,x} \\ 0 & 0 & 0 & 0 & R_{c,y} \end{bmatrix} \quad \text{(C-6a)}$$

$$\mathbf{B}_{g\varsigma c}=\begin{bmatrix}0&0&0&0&R_{c,xx}\\0&0&0&0&R_{c,yy}\\0&0&0&0&R_{c,xy}\end{bmatrix};\mathbf{B}^{g}_{\eta}=\begin{bmatrix}0&0&0&0&\frac{2}{5}R_{c,xx}-\frac{1}{5}R_{c,yy}\\0&0&0&0&-\frac{1}{5}R_{c,xx}+\frac{2}{5}R_{c,yy}\\0&0&0&0&-\frac{2}{5}R_{c,xy}\\0&0&0&0&-\frac{1}{5}R_{c,xx}+\frac{4}{15}R_{c,yy}\\0&0&0&0&\frac{4}{15}R_{c,xx}-\frac{1}{5}R_{c,yy}\\0&0&0&0&\frac{8}{15}R_{c,xy}\\0&0&0&0&-\frac{1}{5}R_{c,xx}-\frac{1}{15}R_{c,yy}\\0&0&0&0&-\frac{1}{15}R_{c,xx}-\frac{1}{5}R_{c,yy}\\0&0&0&0&-\frac{2}{15}R_{c,xy}\end{bmatrix} \tag{C-6b}$$

$$\mathbf{\Lambda}_{\varepsilon}=\begin{bmatrix}w_{,x}&0\\0&w_{,y}\\w_{,y}&w_{,x}\end{bmatrix};\mathbf{\Lambda}_{\varsigma}=\begin{bmatrix}w_{,xx}&w_{,xy}\\w_{,xy}&w_{,yy}\end{bmatrix};\mathbf{\Lambda}_{\eta}=\begin{bmatrix}\frac{2}{5}w_{,xx}-\frac{1}{5}w_{,yy}&-\frac{2}{5}w_{,xy}\\-\frac{2}{5}w_{,xy}&-\frac{1}{5}w_{,xx}+\frac{2}{5}w_{,yy}\\0&0\\\frac{8}{15}w_{,xy}&\frac{4}{15}w_{,xx}-\frac{1}{5}w_{,yy}\\0&0\\-\frac{1}{5}w_{,xx}+\frac{4}{15}w_{,yy}&\frac{8}{15}w_{,xy}\\0&0\\-\frac{1}{5}w_{,xx}-\frac{1}{15}w_{,yy}&-\frac{2}{15}w_{,xy}\\0&0\\-\frac{2}{15}w_{,xy}&-\frac{1}{15}w_{,xx}-\frac{1}{5}w_{,yy}\end{bmatrix} \tag{C-7}$$

$$\hat{\mathbf{N}}_{\varepsilon}=\begin{bmatrix}N_x&N_{xy}\\N_{xy}&N_y\end{bmatrix};\hat{\mathbf{N}}_{th}=\begin{bmatrix}N^{\varepsilon}_{tx}&N^{\varepsilon}_{txy}\\N^{\varepsilon}_{txy}&N^{\varepsilon}_{ty}\end{bmatrix};\hat{\mathbf{N}}_{\varsigma}=\begin{bmatrix}N^{\varsigma}_{x}&0&N^{\varsigma}_{y}\\0&N^{\varsigma}_{y}&N^{\varsigma}_{x}\end{bmatrix} \tag{C-8a}$$

$$\hat{\mathbf{N}}_{\eta}=\begin{bmatrix}N^{\eta}_{xxx}&0&N^{\eta}_{yyy}&3N^{\eta}_{xyy}&0&3N^{\eta}_{xxy}&3N^{\eta}_{xzz}&0&3N^{\eta}_{yzz}\\0&N^{\eta}_{yyy}&N^{\eta}_{xxx}&0&3N^{\eta}_{xxy}&3N^{\eta}_{xyy}&0&3N^{\eta}_{yzz}&3N^{\eta}_{xzz}\end{bmatrix} \tag{C-8b}$$

References

[1] Koizumi M. The concept of FGM. Ceramic Transactions, Functionally Gradient Materials 1993;34:3–10.

[2] Reddy JN. Analysis of functionally graded plates. Int. J. Numer. Methods Eng. 2000;47:663–684.

[3] Praveen GN, Reddy JN. Nonlinear transient thermoelastic analysis of functionally graded ceramic-metal plates. Int. J. Solids Struct. 1998;35:4457–4476.

[4] Ma LS, Wang TJ. Nonlinear bending and post-buckling of a functionally graded circular plate under mechanical and thermal loadings. Int. J. Solids Struct. 2003;40:3311–3330.

[5] Yanga J, Shen HS. Non-linear analysis of functionally graded plates under transverse and in-plane loads. Int. J. Non Linear Mech. 2003;38:467–482.

[6] Na KS, Kim JH. Thermal postbuckling investigations of functionally graded plates using 3-D finite element method. Finite Elem. Anal. Des. 2006;42:749–756.

[7] Park JS, Kim JH. Thermal postbuckling and vibration analyses of functionally graded plates. J. Sound Vib. 2006;289:77–93.

[8] Li SR, Zhang JH, Zhao YG. Nonlinear thermomechanical post-buckling of circular FGM plate with geometric imperfection. Thin Walled Struct. 2007;45:528–536.

[9] Shen HS. Thermal postbuckling behavior of shear deformable FGM plates with temperature-dependent properties. Int. J. Mech. Sci. 2007;49:466–478.

[10] Prakash T, Singha MK, Ganapathi M. Thermal postbuckling analysis of FGM skew plates. Eng. Struct. 2008;30:22–32.

[11] Lee YY, Zhao X, Reddy JN. Postbuckling analysis of functionally graded plates subject to compressive and thermal loads. Comput. Meth. Appl. Mech. Eng. 2010;199:1645–1653.

[12] Asemi K, Salehi M, Akhlaghi M. Post-buckling analysis of FGM annular sector plates based on three dimensional elasticity graded finite elements. Int. J. Non Linear Mech. 2014;67:164–177.

[13] Ovesy HR, Ghannadpour SAM, Nassirnia M. Post-buckling analysis of rectangular plates comprising Functionally Graded Strips in thermal environments. Comput. Struct. 2015;147:209–215.

[14] Zhang DG, Zhou HM. Mechanical and thermal post-buckling analysis of FGM rectangular plates with various supported boundaries resting on nonlinear elastic foundations. Thin Walled Struct. 2015;89:142–151.

[15] Zhang LW, Liew KM, Reddy JN. Postbuckling behavior of bi-axially compressed arbitrarily straight-sided quadrilateral functionally graded material plates. Comput. Meth. Appl. Mech. Eng. 2016;300:593–610.

[16] Tran LV, Phung-Van P, Lee J, Wahab MA, Nguyen-Xuan H. Isogeometric analysis for nonlinear thermomechanical stability of functionally graded plates. Compos. Struct. 2016;140:655–667.

[17] Taczaa M, Buczkowski R, Kleiber M. Nonlinear buckling and post-buckling response of stiffened FGM plates in thermal environments. Compos Part B: Eng. 2017;109:238–247.

[18] Zhang DG. Thermal post-buckling analysis of functionally graded material elliptical plates based on high-order shear deformation theory. Mech. Adv. Mater. Struct. 2017;24:142–148.

[19] Thai HT, Kim SE. A review of theories for the modeling and analysis of functionally graded plates and shells. Compos. Struct. 2015;128:70–86.

[20] Swaminathan K, Sangeetha DM. Thermal analysis of FGM plates A critical review of various modeling techniques and solution methods. Compos. Struct. 2017;160:43–60.

[21] Witvrouw A, Mehta A. The use of functionally graded poly-SiGe layers for MEMS applications. Mater. Sci. Forum 2005;492-493:255–260.

[22] Thai HT, Vo TP, Nguyen TK, Kim SE. A review of continuum mechanics models for size-dependent analysis of beams and plates. Compos. Struct. 2017;177:196–219.

[23] Eringen A. Nonlocal polar elastic continua. Int. J. Eng. Sci. 1972;10:1–16. .

[24] Yang F, Chong A, Lam D, Tong P. Couple stress based strain gradient theory for elasticity. Int. J. Solids Struct. 2002;39:2731–2743.

[25] Lam DCC, Yang F, Chong ACM, Wang J, Tong P. Experiments and theory in strain gradient elasticity. J. Mech. Phys. Solids 2003;51:1477–1508.

[26] Shen JP, Li C. A semi-continuum-based bending analysis for extreme-thin micro/nano-beams and new proposal for nonlocal differential constitution. Compos. Struct. 2017;172:210–220.

[27] Li C, Liu JJ, Cheng M, Fan XL. Nonlocal vibrations and stabilities in parametric resonance of axially moving viscoelastic piezoelectric nanoplate subjected to thermo-electro-mechanical forces. Compos Part B: Eng. 2017;116:153–169.

[28] Li C, Li S, Yao L, Zhu Z. Nonlocal theoretical approaches and atomistic simulations for longitudinal free vibration of nanorods/nanotubes and verification of different nonlocal models. Appl. Math. Modell. 2015;39(15):4570–4585.

[29] Li C, Yao L, Chen W, Li S. Comments on nonlocal effects in nano-cantilever beams. Int. J. Eng. Sci. 2015;87:47–57.

[30] Nguyen NT, Hui D, Lee J, Nguyen-Xuan H. An efficient computational approach for size-dependent analysis of functionally graded nanoplates. Comput. Meth. Appl. Mech. Eng. 2015;297:191–218.

[31] Phung-Van P, Ferreira AJM, Nguyen-Xuan H, Abdel Wahab M. An isogeometric approach for size-dependent geometrically nonlinear transient analysis of functionally graded nanoplates. Compos Part B: Eng. 2017;118:125–134.

[32] Park SK, Gao XL. Bernoulli–euler beam model based on a modified couple stress theory. J. Micromech. Microeng. 2006;16:2355.

[33] Ma HM, Gao XL, Reddy JN. A microstructure-dependent timoshenko beam model based on a modified couple stress theory. J. Mech. Phys. Solids 2008;56:3379–3391.

[34] Ma HM, Gao XL, Reddy JN. A nonclassical reddy-levinson beam model based on a modified couple stress theory. Int. J. Multiscale Comput. Eng. 2010;8:167–180.

[35] Ma HM, Gao XL, Reddy JN. A non-classical mindlin plate model based on a modified couple stress theory. Acta Mech. 2011;220:217–235.

[36] Reddy JN. Microstructure-dependent couple stress theories of functionally graded beams. J. Mech. Phys. Solids 2011;59:2382–2399.

[37] Gao XL, Huang JX, Reddy JN. A non-classical third-order shear deformation plate model based on a modified couple stress theory. Acta Mech. 2013;224:2699–2718.

[38] Arbind A, Reddy JN. Nonlinear analysis of functionally graded microstructure-dependent beams. Compos. Struct. 2013;98:272–281.

[39] Arbind A, Reddy JN, Srinivasa AR. Modified couple stress-based third-order theory for nonlinear analysis of functionally graded beams. Latin American Journal of Solids and Structures 2014;11:459–487.

[40] Reddy JN, Srinivasa AR. Non-linear theories of beams and plates accounting for moderate rotations and material length scales. Int. J. Non Linear Mech. 2014;66:43–53.

[41] Reddy JN, Kim J. A nonlinear modified couple stress-based third-order theory of functionally graded plates. Compos. Struct. 2012;94:1128–1143.

[42] Kim J, Reddy JN. Analytical solutions for bending, vibration, and buckling of fgm plates using a couple stress-based third-order theory. Compos. Struct. 2013;103:86–98.

[43] Kim J, Reddy JN. A general third-order theory of functionally graded plates with modified couple stress effect and the von kármán nonlinearity: theory and finite element analysis. Acta Mech. 2015;226:1–26.

[44] Nguyen HX, Nguyen TN, Abdel-Wahab M, Bordas SPA, Nguyen-Xuan H, Vo TP. A refined quasi-3d isogeometric analysis for functionally graded microplates based on the modified couple stress theory. Comput. Meth. Appl. Mech. Eng. 2017;313:904–940.

[45] Ke LL, Yang J, Kitipornchai S, Bradford MA. Bending, buckling and vibration of size-dependent functionally graded annular microplates. Compos. Struct. 2012;94(11):3250–3257.

[46] Ke LL, Yang J, Kitipornchai S, Bradford MA, Wang YS. Axisymmetric nonlinear free vibration of size-dependent functionally graded annular microplates. Compos Part B: Eng. 2013;53:207–217.

[47] Ke LL, Wang YS, Yang J, Kitipornchai S. Nonlinear free vibration of size-dependent functionally graded microbeams. Int. J. Eng. Sci. 2012;50(1):256–267.

[48] Reddy JN, Romanoff J, Loya JA. Nonlinear finite element analysis of functionally graded circular plates with modified couple stress theory. Eur. J. Mech. A. Solids 2016;56:92–104.

[49] Mindlin R. Second gradient of strain and surface-tension in linear elasticity. Int. J. Solids Struct. 1965;1:417–438.

[50] Wang B, Zhou S, Zhao J, Chen X. A size-dependent Kirchhoff micro-plate model based on strain gradient elasticity theory. Eur. J. Mech. A. Solids 2011;30:517–524.

[51] Ashoori Movassagh A, Mahmoodi MJ. A micro-scale modeling of Kirchhoff plate based on modified strain-gradient elasticity theory. Eur. J. Mech. A. Solids 2013;40:50–59.

[52] Sahmani S, Ansari R. On the free vibration response of functionally graded higher-order shear deformable microplates based on the strain gradient elasticity theory. Compos. Struct. 2013;95:430–442.

[53] Li A, Zhou S, Zhou S, Wang B. A size-dependent model for bi-layered Kirchhoff micro-plate based on strain gradient elasticity theory. Compos. Struct. 2014;113:272–280.

[54] Ansari R, Gholami R, Faghih Shojaei M, Mohammadi V, Sahmani S. Bending, buckling and free vibration analysis of size-dependent functionally graded circular/annular microplates based on the modified strain gradient elasticity theory. Eur. J. Mech. A. Solids 2015;49:251–267.

[55] Zhang B, He Y, Liu D, Lei J, Shen L, Wang L. A size-dependent third-order shear deformable plate model incorporating strain gradient effects for mechanical analysis of functionally graded circular/annular microplates. Compos Part B: Eng. 2015;79:553–580.

[56] Zhang B, He Y, Liu D, Shen L, Lei J. An efficient size-dependent plate theory for bending, buckling and free vibration analyses of functionally graded microplates resting on elastic foundation. Appl. Math. Modell. 2015;39:3814–3845.

[57] Mirsalehi M, Azhari M, Amoushahi H. Buckling and free vibration of the FGM thin micro-plate based on the modified strain gradient theory and the spline finite strip method. Eur. J. Mech. A. Solids 2017;61:1–13.

[58] Hosseini M, Bahreman M, Jamalpoor A. Using the modified strain gradient theory to investigate the size-dependent biaxial buckling analysis of an orthotropic multi-microplate system. Acta Mech. 2016;227:1621–1643.

[59] Thai S, Thai HT, Vo TP, Patel VI. Size-dependant behaviour of functionally graded microplates based on the modified strain gradient elasticity theory and isogeometric analysis. Comput. Struct. 2017;190:219–241.

[60] Ansari R, Gholami R, Shojaei MF, Mohammadi V, Darabi MA. Thermal Buckling Analysis of a Mindlin Rectangular FGM Microplate Based on the Strain Gradient Theory. J. Therm. Stresses 2013;36:446–465.

[61] Shenas AG, Malekzadeh P. Free vibration of functionally graded quadrilateral microplates in thermal environment. Thin Walled Struct. 2016;106:294–315.

[62] Emami AA, Alibeigloo A. Thermoelastic damping analysis of FG Mindlin microplates using strain gradient theory. J. Therm. Stresses 2016;39:1499–1522.

[63] Hughes TJR, Cottrell JA, Bazilevs Y. Isogeometric analysis: CAD, finite elements, NURBS, exact geometry and mesh refinement. Comput. Meth. Appl. Mech. Eng. 2005;194:4135–4195.

[64] Nguyen VP, Anitescu C, Bordas SPA, Rabczuk T. Isogeometric analysis: An overview and computer implementation aspects. Math. Comput. Simul 2015;117:89–116.

[65] Reddy JN. A simple higher-order theory for laminated composite plates. J. Appl. Mech. 1984;51:745–752.

[66] Touloukian, Gerristen Y, Moore JaNY. Thermophysical properties research literature retrieval guide. 2d ed. rev and expanded ed. , New York : Plenum Press , 1967.

[67] Malekzadeh P, Monajjemzadeh SM. Dynamic response of functionally graded beams in a thermal environment under a moving load. Mech. Adv. Mater. Struct. 2016;23:248–258.

[68] Taati E, Molaei Najafabadi M, Reddy JN. Size-dependent generalized thermoelasticity model for Timoshenko micro-beams based on strain gradient and non-Fourier heat conduction theories. Compos. Struct. 2014;116:595–611.

[69] Piegl L, Tiller W. The NURBS Book. Monographs in Visual Communications , Berlin, Heidelberg: Springer Berlin Heidelberg , 1995.

[70] Cottrell JA, Hughes TJR, Bazilevs Y. Isogeometric Analysis: Toward Integration of CAD and FEA. 1st ed. , Wiley Publishing , 2009.

[71] Liew KM, Wang J, Tan MJ, Rajendran S. Postbuckling analysis of laminated composite plates using the mesh-free kp-Ritz method. Computer Methods in Applied Mechanics and Engineering 2006;195:551–570.

[72] Le-Manh T, Lee J. Postbuckling of laminated composite plates using NURBS-based isogeometric analysis. Compos. Struct. 2014;109:286–293.

Table 1: Material properties of temperature-independent FGMs

	E (Pa)	α (1/K)	κ (W/mK)	ν
Al	7.0e10	23.0	204	0.3
Al2O3	3.8e11	7.2	10.4	0.3

Table 2: Material properties of temperature-dependent FGMs

Materials	Proprieties	P_0	P_{-1}	P_1	P_2	P_3
Si3N4	E (Pa)	3.4843e11	0	-3.070e-04	2.160e-07	-8.946e-11
	α (1/K)	5.8723e-06	0	9.095e-04	0	0
	κ (W/mK)	13.723	0	-1.032e-03	5.466e-07	-7.876e-11
	ν	0.24	0	0	0	0
SUS304	E (Pa)	2.0104e11	0	3.079e-04	-6.534e-07	0
	α (1/K)	1.2330e-05	0	8.086e-04	0	0
	κ (W/mK)	15.379	0	-1.264e-03	2.092e-06	-7.223e-10
	ν	0.3262	0	-2.002e-04	3.797e-07	0

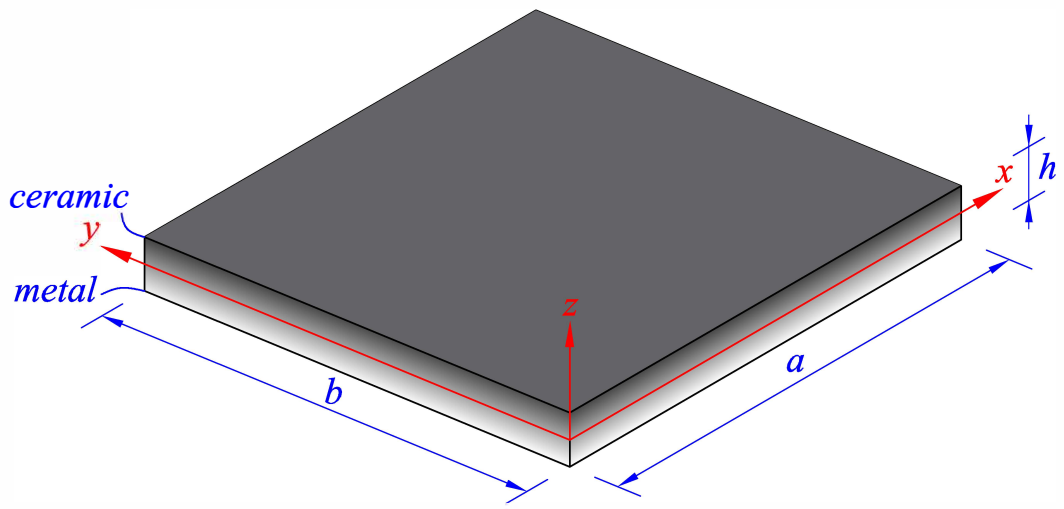

Figure 1: Configuration of a rectangular FG plate

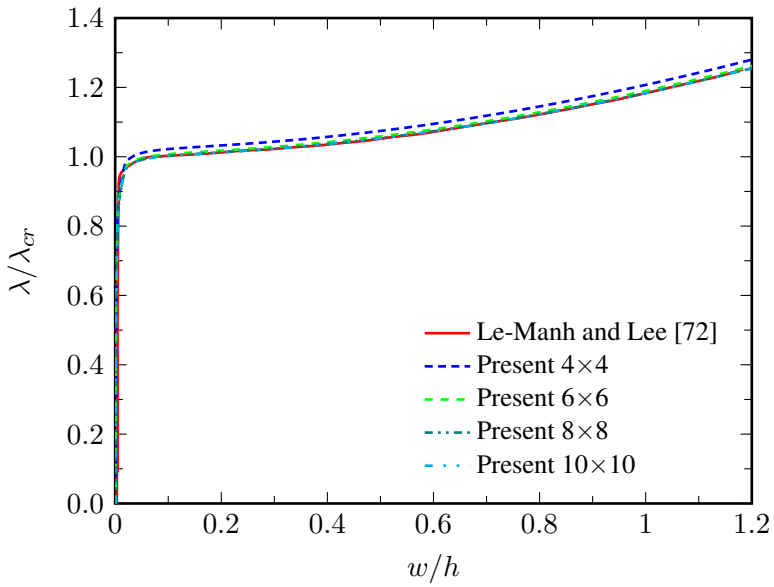

Figure 2: Post-buckling path of a square SSSS1$_m$ isotropic plate under uniaxial compression (a/h = 50)

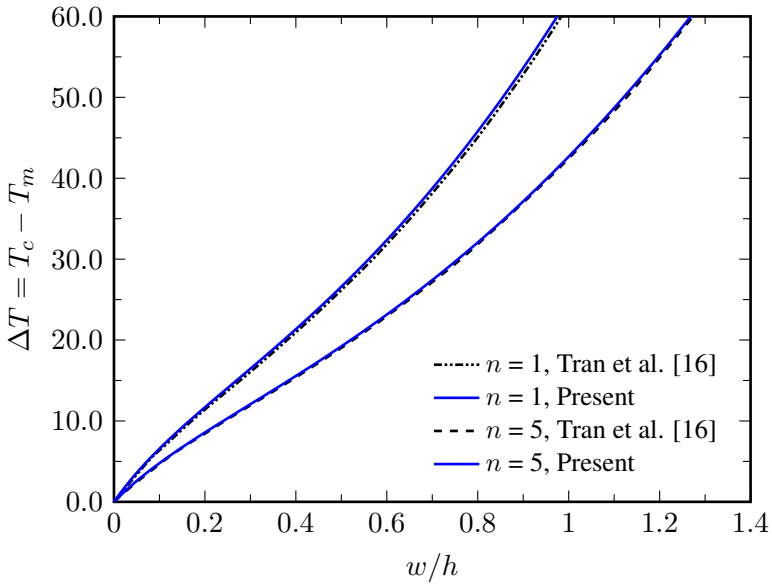

Figure 3: Post-buckling paths of square SSSS2$_t$ Al2O3/Al plates under nonlinear temperature rise (a/h = 100)

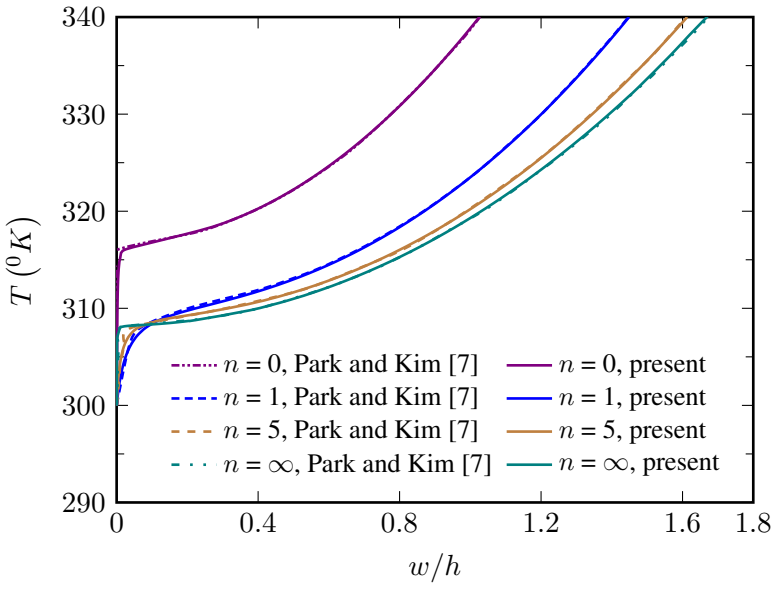

Figure 4: Post-buckling paths of square SSSS2$_t$ Si3N43/SU3S304 plates under uniform temperature rise (a/h = 100)

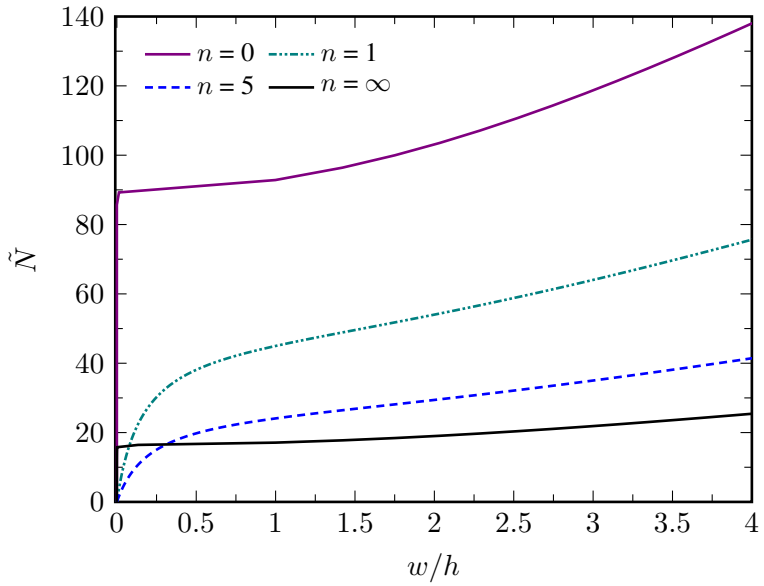

Figure 5: Influence of gradient indices n on the post-buckling behavior of square SSSS1$_m$ Al2O3/Al microplates under uniaxial compression $(a/h = 20,\ h/l = 2)$

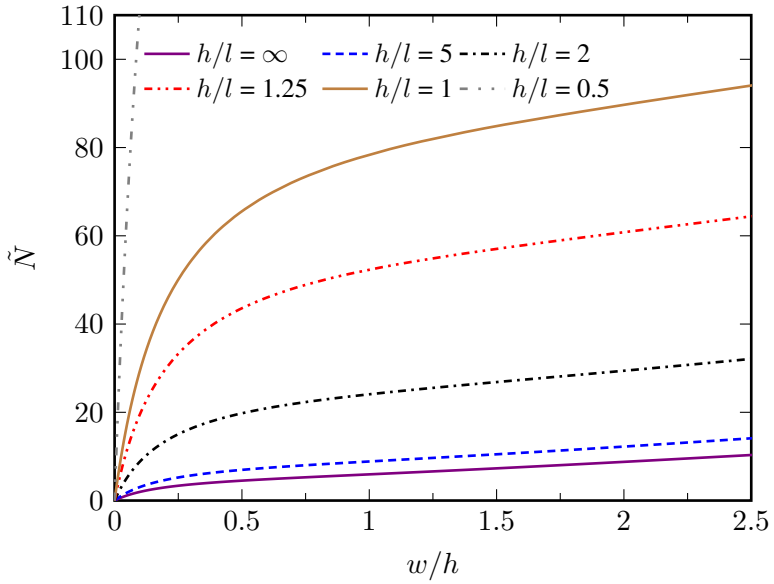

Figure 6: Influence of size effects on the post-buckling behavior of square SSSS1$_m$ Al2O3/Al microplates under uniaxial compression $(a/h = 20,\ n = 5)$

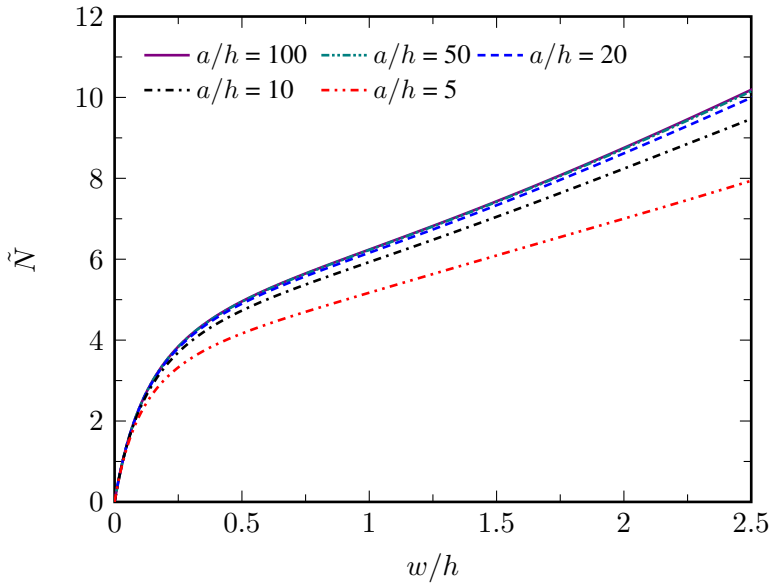

Figure 7: Influence of thickness ratios on the post-buckling behavior of square SSSS1$_m$ Al2O3/Al microplates under uniaxial compression load ($h/l = 10$, $n = 10$)

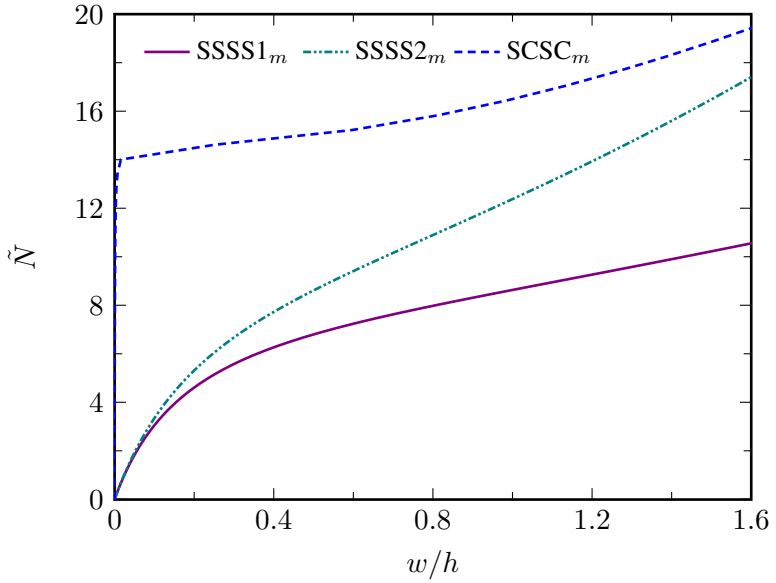

Figure 8: Influence of boundary conditions on the post-buckling behavior of square Al2O3/Al microplates under uniaxial compression ($h/l = 5$, $n = 5$, $a/h = 10$)

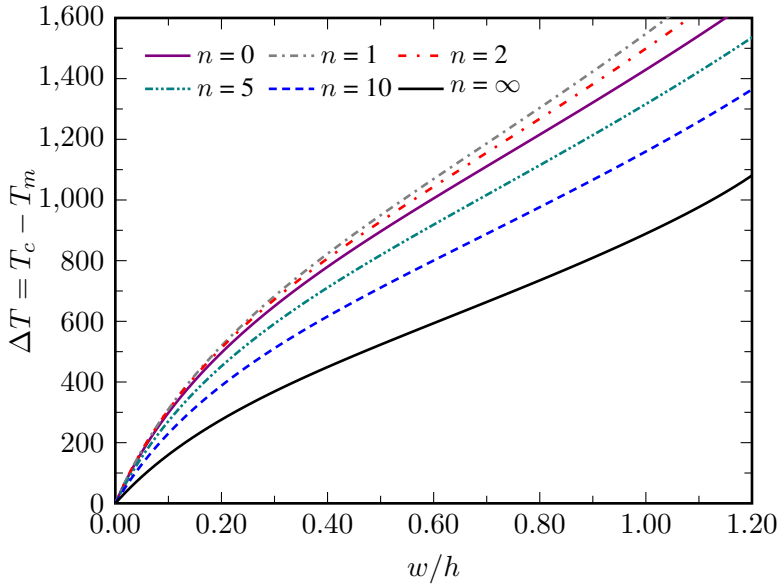

Figure 9: Influence of gradient indices n on the post-buckling behavior of square SSSS1$_t$ Si3N4/SU3S304 microplates subjected to thermal loading ($a/h = 20$, $h/l = 10$)

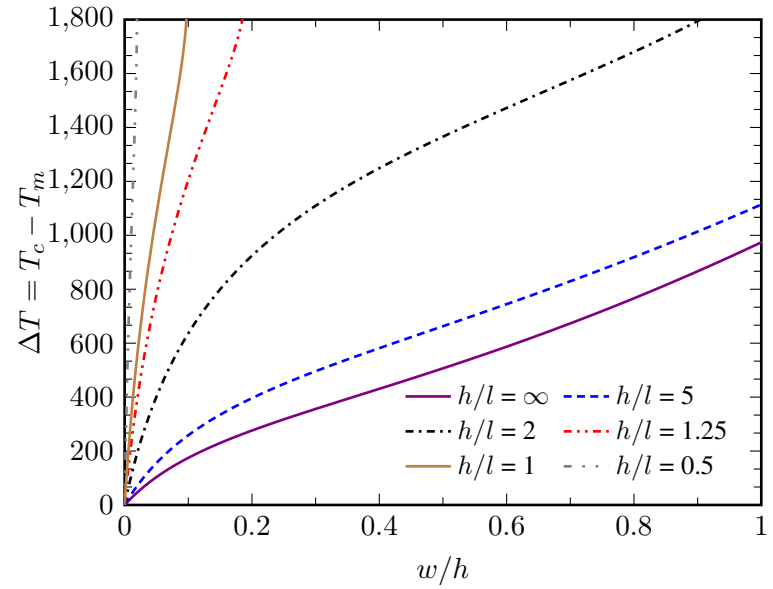

Figure 10: Influence of size effects on the post-buckling behavior of square SSSS2$_t$ Si3N4/SU3S304 microplates subjected to thermal loading ($a/h = 20$, $n = 5$)

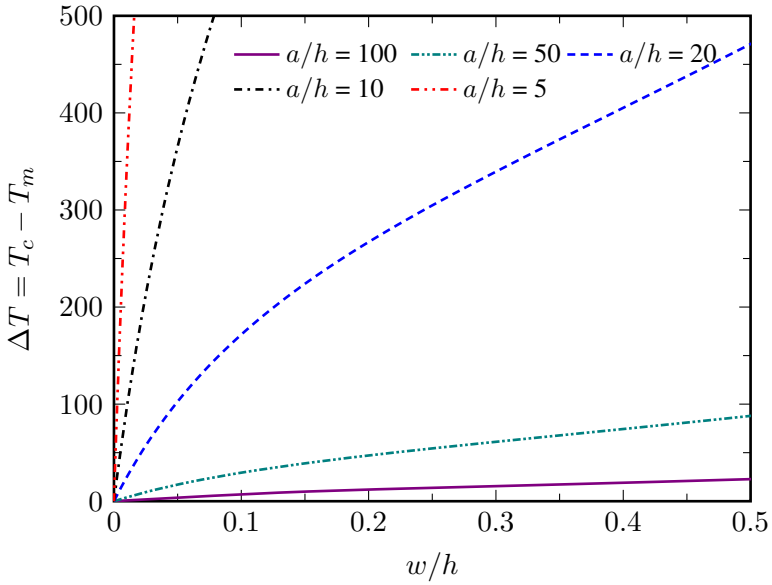

Figure 11: Influence of thickness ratios on the post-buckling behavior of square SSSS2$_m$ Si3N4/SU3S304 microplates subjected to thermal loading ($h/l = 10$, $n = 10$)

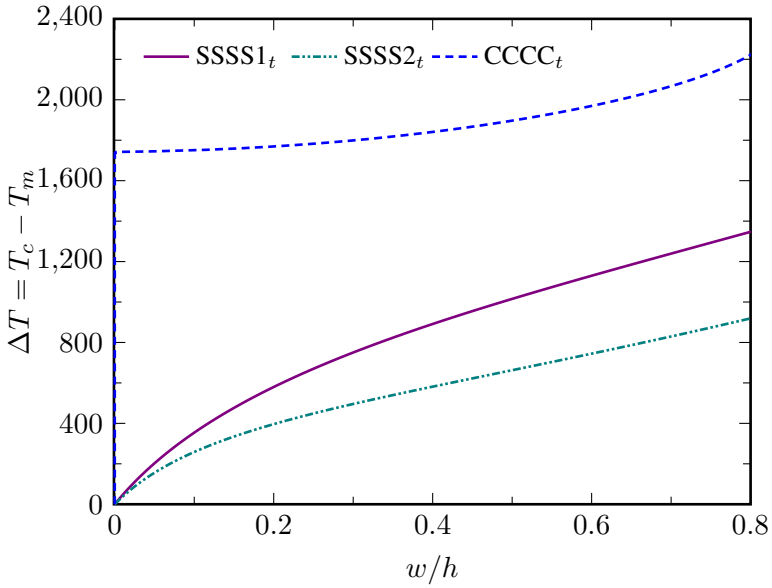

Figure 12: Influence of boundary conditions on the post-buckling behavior of square Si3N4/SU3S304 microplates subjected to thermal loading ($h/l = 5$, $n = 5$, $a/h = 20$)